averaged for eight dogs in a previous study was 1.65 at the beginning of the ejection phase.[19] At the end of the ejection phase, the ratio increased to 1.88. If these values are translated into α in equation 1, α increases from 1.73 to 1.89 (a net increase of 10%) during the ejection phase. Hence, α is actually not constant within one animal. Although this can be a confounder in this theoretical analysis (Appendix), its effect would be quantitatively small. Apart from α, the time-varying LV elastance, $E(t)$, also determines S_m (equation A9 in Appendix). If $E(t)$ is constant, S_m is achieved when α is maximum, that is, at the end of the ejection phase. Meanwhile, if α is constant, S_m is achieved when $E(t)$ is minimum, that is, at the beginning of the ejection phase. During the ejection phase, $E(t)$ increases from 5 to 10 mm Hg/mL in dogs (a net increase of 100%).[15] A numerical simulation using these published data indicates that the contribution of $E(t)$ to S_m is 15 times more than that of α. Thus, we can assume α as constant without sacrificing accuracy. S_m is effectively determined by $E(t)$ and is achieved at the beginning of the ejection phase. This is compatible with in vivo findings. In this study (Figures 2B, 2C, and 3B) and also in previous studies,[4,7,23] S_m is usually reached early in the ejection phase.

According to the value of R^2, the theoretical model can predict 79% of S_m variation. The residual variation, 21%, remains to be explained. Although it is possible that variation among animals of α in equation 1 may contribute to this residual variation, the CV of α in eight dogs was <5% in a previous study,[19] suggesting that variation among animals of α plays a minor role in the residual variation. The variation may be caused by factors not included in the model. A previous study indicated that dynamic arterial properties such as aortic compliance have direct effects on S_m.[10] Further studies to address these issues are required in the future.

LV contractility determines the magnitude of S_m. The R^2 value of 0.64 between S_m and E_{es}' in this study was comparable with those observed between S_m and other LV functional indexes, such as LV dP/dt_{max}, in previous studies.[7] Borlaug *et al.*[9] reported that S_m was not correlated with indexes of LV contractility including, E_{es}', in patients with hypertension. However, because they excluded patients with heart failure with depressed LV contractility from the study population and did not actively stimulate LV inotropy in their protocol, LV contractile indexes were well preserved with small variations among patients. This might be a reason they did not detect a significant correlation between S_m and indexes of LV contractility.

S_m is inversely related to LV afterload. Previous clinical studies have yielded contrasting results of dependence[9,10,24] and independence[11,25] of S_m on afterload. Oki *et al.*[24] reported that S_m was reduced in response to an increase in LV afterload after angiotensin infusion in healthy subjects. In contrast, Amà *et al.*[11] reported that S_m did not change when E_a and SVR were changed by phenylephrine or nitroglycerine infusion in patients undergoing cardiac surgery. However, they did not attempt to directly associate S_m with the afterload indexes. Similar to their results, we also noted that S_m did not change in response to phenylephrine infusion, whereas E_a or SVR significantly increased (Table 1). However, we further analyzed the associations between S_m and afterload indexes using mixed-model procedures. In the previous studies, conducting statistical analyses similar to those we performed in this study would have been useful to evaluate association between the afterload and S_m.

Unexpectedly, V_{ed} and EJT did not affect S_m independently. Both V_{ed} and EJT are components of our theoretical model of S_m. Furthermore, previous studies suggested that S_m was affected by LV preload and EJT.[23,26] In this study, the CVs for $V_{ed}^{1/3}$ and EJT^{-1} were small compared with those for E_{es}' and E_a^{-1}. Moreover, E_{es}' was correlated inversely with $V_{ed}^{1/3}$, and E_a^{-1} was correlated inversely with EJT^{-1}. These suggest that because of the low variability of $V_{ed}^{1/3}$ and EJT^{-1} and the antagonizing effects of the covariates (E_{es}' and E_a^{-1}), the analysis might fail to detect significant correlations of $V_{ed}^{1/3}$ and EJT^{-1} with S_m. However, V_{ed} also was not correlated with S_m in this study (data not shown), although the CVs for V_{ed} and E_{es}' were comparable (41% and 49%). It would be ideal to change V_{ed} or EJT individually while keeping all other parameters constant. Although impedance loading on ex vivo heart preparation would realize such protocols,[8] this preparation is inappropriate for the study of LV longitudinal function, because it requires resection of the mitral valve and subvalvular apparatus (papillary muscles), which are critical components of longitudinal function.[27] Taken together, although we cannot completely exclude significant contributions of LV preload and EJT to S_m, their effects may be small and easily reversed by the effects of LV contractility and afterload, that is, effectively negligible compared with the status of ventricular-arterial coupling.

Potential Clinical Implications

A novel and important finding of this study is that S_m strongly reflects the status of ventricular-arterial coupling. Ventricular-arterial coupling is a central determinant of cardiovascular performance and cardiac energetics.[13-15,28,29] Normally, the left ventricle and the arterial system are optimally coupled to produce maximal stroke work, when E_{es}/E_a is near unity. Maximal energetic efficiency occurs when E_{es}/E_a approximates 2.0. In patients with heart failure, the left ventricle and the arterial system are suboptimally coupled (E_{es}/E_a becomes less than unity). Beta-blockade improves this situation.[20] In patients with myocardial infarction, suboptimal coupling ratio is associated with poor prognosis over the next 5 years.[29] S_m as a measure of the status of ventricular-arterial coupling may allow accurate evaluations of cardiovascular pathophysiology and also predictions of prognosis in patients with cardiac disease. The ventricular-arterial coupling ratio can be predicted also by LVEF.[8] However, LVEF assessment requires precise definition of the endocardial borders on conventional echocardiography, which is complicated by trabeculae or endocardial dropout. Precise endocardial definition is sometimes difficult, especially in obese patients, the elderly, and patients with pulmonary disease. Recording of mitral annular motion has the advantage that it is not dependent on the endocardial definition and is therefore relatively independent of image quality.[7] S_m measurement can be an alternative to LVEF assessment to predict the status of ventricular-arterial coupling in such patients.

Study Limitations

In accordance with a previous canine study,[17] sonomicrometry consistently underestimated systolic mitral annular velocity compared with TD echocardiography (Figure 2D). This discrepancy may be attributed to the location of the crystals, which are implanted in the subepicardium. Although longitudinally directed myocardial fibers in both subendocardial and subepicardial layers of the left ventricle may play a major role in the magnitude of systolic mitral annular velocity,[1] systolic shortening of subepicardial fiber is significantly smaller than that of subendocardial fiber.[30] In humans, the absolute value of mitral annular velocity measured by TD echocardiography agreed with that measured by cardiac magnetic resonance imaging, which is the widely accepted gold standard for the assessment of LVV and function.[31] Although sonomicrometry is useful in animal experiments

for the assessment of heart motion, our data suggest that S_m obtained by sonomicrometry in this study might have underestimated the true LV longitudinal shortening velocity. However, a strong correlation was observed between S_m and S_{mTD} (Figure 2D). Percentage changes in S_m and S_{mTD} were also correlated tightly (Figure 2E), indicating that S_m sensitively tracked changes in S_{mTD}. Taken together, it is fair to say that conclusions provided by sonomicrometry in this study are comparable, at least qualitatively, with those obtained by TD echocardiography.

In analyzing the experimental data, we relied on E_{es}' (the P_{es}/V_{es} ratio) to quantify LV contractility, which can be evaluated more precisely by both the slope (E_{es}) and volume axis intercept (V_0) of the relationship between P_{es} and V_{es} (Figure 1A).[12] It was unclear how each contributed to the magnitude of S_m in this study. Despite these limitations, the P_{es}/V_{es} ratio as a single contractile index simplifies the statistical analysis of contractility.[9,20]

Colinearity among the cardiovascular parameters as noted between E_{es}' and $V_{ed}^{1/3}$ might have affected the present results. The colinearity may be attributable to the nature of the protocols, such as heart failure induction, which depresses LV contractility and increases preload simultaneously. However, the protocols are analogous to commonly observed clinical setting or practice, that is, relevant to possible clinical application of the conclusions of this study.

CONCLUSIONS

LV contractility and afterload independently determine S_m. The effects of LV preload and EJT on S_m might be small, even though they are theoretically associated with S_m. S_m strongly reflects the status of ventricular-arterial coupling.

REFERENCES

1. Nikitin NP, Witte KK, Thackray SD, de Silva R, Clark AL, Cleland JG. Longitudinal ventricular function: normal values of atrioventricular annular and myocardial velocities measured with quantitative two-dimensional color Doppler tissue imaging. J Am Soc Echocardiogr 2003;16:906-21.
2. Gulati VK, Katz WE, Follansbee WP, Gorcsan J III. Mitral annular descent velocity by tissue Doppler echocardiography as an index of global left ventricular function. Am J Cardiol 1996;77:979-84.
3. Hori Y, Sato S, Hoshi F, Higuchi S. Assessment of longitudinal tissue Doppler imaging of the left ventricular septum and free wall as an indicator of left ventricular systolic function in dogs. Am J Vet Res 2007;68:1051-7.
4. Mogelvang R, Goetze JP, Pedersen SA, Olsen NT, Marott JL, Schnohr P, et al. Preclinical systolic and diastolic dysfunction assessed by tissue Doppler imaging is associated with elevated plasma pro-B-type natriuretic peptide concentrations. J Card Fail 2009;15:489-95.
5. Nikitin NP, Loh PH, Silva R, Ghosh J, Khaleva OY, Goode K, et al. Prognostic value of systolic mitral annular velocity measured with Doppler tissue imaging in patients with chronic heart failure caused by left ventricular systolic dysfunction. Heart 2006;92:775-9.
6. Mogelvang R, Sogaard P, Pedersen SA, Olsen NT, Marott JL, Schnohr P, et al. Cardiac dysfunction assessed by echocardiographic tissue Doppler imaging is an independent predictor of mortality in the general population. Circulation 2009;119:2679-85.
7. Seo JS, Kim DH, Kim WJ, Song JM, Kang DH, Song JK. Peak systolic velocity of mitral annular longitudinal movement measured by pulsed tissue Doppler imaging as an index of global left ventricular contractility. Am J Physiol Heart Circ Physiol 2010;298:H1608-15.
8. Kass DA, Maughan WL, Guo ZM, Kono A, Sunagawa K, Sagawa K. Comparative influence of load versus inotropic states on indexes of ventricular contractility: experimental and theoretical analysis based on pressure-volume relationships. Circulation 1987;76:1422-36.
9. Borlaug BA, Melenovsky V, Redfield MM, Kessler K, Chang HJ, Abraham TP, et al. Impact of arterial load and loading sequence on left ventricular tissue velocities in humans. J Am Coll Cardiol 2007;50:1570-7.
10. Henein MY, Das SK, O'Sullivan C, Kakkar VV, Gillbe CE, Gibson DG. Effect of acute alterations in afterload on left ventricular function in patients with combined coronary artery and peripheral vascular disease. Heart 1996;75:151-8.
11. Amà R, Segers P, Roosens C, Claessens T, Verdonck P, Poelaert J. The effects of load on systolic mitral annular velocity by tissue Doppler imaging. Anesth Analg 2004;99:332-8.
12. Burkhoff D, Mirsky I, Suga H. Assessment of systolic and diastolic ventricular properties via pressure-volume analysis: a guide for clinical, translational, and basic researchers. Am J Physiol Heart Circ Physiol 2005;289:H501-12.
13. Sunagawa K, Maughan WL, Burkhoff D, Sagawa K. Left ventricular interaction with arterial load studied in isolated canine ventricle. Am J Physiol Heart Circ Physiol 1983;245:H773-80.
14. Hayashi K, Shigemi K, Shishido T, Sugimachi M, Sunagawa K. Single-beat estimation of ventricular end-systolic elastance-effective arterial elastance as an index of ventricular mechanoenergetic performance. Anesthesiology 2000;92:1769-76.
15. Shishido T, Hayashi K, Shigemi K, Sato T, Sugimachi M, Sunagawa K. Single-beat estimation of end-systolic elastance using bilinearly approximated time-varying elastance curve. Circulation 2000;102:1983-9.
16. National Institutes of Health. Guide for the care and use of laboratory animals (NIH Publication No. 85-23). Bethesda, MD: National Institutes of Health; 1996.
17. Opdahl A, Remme EW, Helle-Valle T, Lyseggen E, Vartdal T, Pettersen E, et al. Determinants of left ventricular early-diastolic lengthening velocity: independent contributions from left ventricular relaxation, restoring forces, and lengthening load. Circulation 2009;119:2578-86.
18. Ratcliffe MB, Gupta KB, Streicher JT, Savage EB, Bogen DK, Edmunds LH Jr. Use of sonomicrometry and multidimensional scaling to determine the three-dimensional coordinates of multiple cardiac locations: feasibility and initial implementation. IEEE Trans Biomed Eng 1995;42:587-98.
19. Rankin JS, McHale PA, Arentzen CE, Ling D, Greenfield JC Jr., Anderson RW. The three-dimensional dynamic geometry of the left ventricle in the conscious dog. Circ Res 1976;39:304-13.
20. Maurer MS, Sackner-Bernstein JD, El-Khoury Rumbarger L, Yushak M, King DL, Burkhoff D. Mechanisms underlying improvements in ejection fraction with carvedilol in heart failure. Circ Heart Fail 2009;2:189-96.
21. Colin P, Ghaleb B, Monnet X, Hittinger L, Berdeaux A. Effect of graded heart rate reduction with ivabradine on myocardial oxygen consumption and diastolic time in exercising dogs. J Pharmacol Exp Ther 2004;308:236-40.
22. Fitzmaurice GM, Ravichandran C. A primer in longitudinal data analysis. Circulation 2008;118:2005-10.
23. Odland HH, Kro GA, Munkeby BH, Edvardsen T, Saugstad OD, Thaulow E. Ejection time-corrected systolic velocity improves accuracy in the evaluation of myocardial dysfunction: a study in piglets. Pediatr Cardiol 2010;31:1070-8.
24. Oki T, Fukuda K, Tabata T, Mishiro Y, Yamada H, Abe M, et al. Effect of an acute increase in afterload on left ventricular regional wall motion velocity in healthy subjects. J Am Soc Echocardiogr 1999;12:476-83.
25. Palmieri V, Russo C, Arezzi E, Pezzullo S, Sabatella M, Minichiello S, et al. Relations of longitudinal left ventricular systolic function to left ventricular mass, load, and Doppler stroke volume. Eur J Echocardiogr 2006;7:348-55.
26. Pelà G, Regolisti G, Coghi P, Cabassi A, Basile A, Cavatorta A, et al. Effects of the reduction of preload on left and right ventricular myocardial velocities analyzed by Doppler tissue echocardiography in healthy subjects. Eur J Echocardiogr 2004;5:262-71.

27. Jones CJ, Raposo L, Gibson DG. Functional importance of the long axis dynamics of the human left ventricle. Br Heart J 1990;63:215-20.
28. Burkhoff D, Sagawa K. Ventricular efficiency predicted by an analytical model. Am J Physiol 1986;250:R1021-7.
29. Antonini-Canterin F, Enache R, Popescu BA, Popescu AC, Ginghina C, Leiballi E, et al. Prognostic value of ventricular-arterial coupling and B-type natriuretic peptide in patients after myocardial infarction: a five-year follow-up study. J Am Soc Echocardiogr 2009;22:1239-45.
30. Sabbah HN, Marzilli M, Stein PD. The relative role of subendocardium and subepicardium in left ventricular mechanics. Am J Physiol 1981;240:H920-6.
31. Marsan NA, Westenberg JJ, Tops LF, Ypenburg C, Holman ER, Reiber JH, et al. Comparison between tissue Doppler imaging and velocity-encoded magnetic resonance imaging for measurement of myocardial velocities, assessment of left ventricular dyssynchrony, and estimation of left ventricular filling pressures in patients with ischemic cardiomyopathy. Am J Cardiol 2008;102:1366-72.

APPENDIX

Instantaneous LVP, P(*t*), and LVV, V(*t*), are related by the following formula:

$$V(t) = \frac{P(t)}{E(t)} + V_0, \tag{A2}$$

where E(*t*) is time-varying LV elastance and V_0 is the volume axis intercept of the relationship between P_{es} and V_{es}.[12] S_m is a parameter of the ejection phase. The left ventricle has an ellipsoid shape, and the ratio of LV longitudinal length, L(*t*), to short-axis length is assumed to be constant during the ejection phase. L(*t*) and its time derivative are expressed as follows:

$$L(t) = \alpha[V(t)]^{1/3}, \tag{A3}$$

$$dL(t)/dt = \frac{\alpha}{3} \cdot dV(t)/dt \cdot [V(t)]^{-2/3}. \tag{A4}$$

During the ejection phase, because P(*t*) can be approximated to P_{es} (Figure 1A), equation A2 is rewritten as follows:

$$V(t) = \frac{P_{es}}{E(t)} + V_0. \tag{A5}$$

Differentiation of both sides of equation A5 with respect to time yields

$$dV(t)/dt = \frac{-P_{es} \cdot dE(t)/dt}{[E(t)]^2}. \tag{A6}$$

During the ejection phase, because E(*t*) increases linearly with respect to time,[14,15] dE(*t*)/dt is expressed as follows (Figure 1B):

$$dE(t)/dt = \frac{E_{es} - E_{ad}}{EJT}, \tag{A7}$$

where E_{ad} is the elastance value at the end of the isovolumic contraction phase (Figure 1B).[14,15] Substituting equation A7 into equation A6 yields

$$dV(t)/dt = \frac{-P_{es}}{[E(t)]^2 \cdot EJT} \cdot (E_{es} - E_{ad}). \tag{A8}$$

Substituting equations A5 and A8 into equation A4 yields

$$dL(t)/dt = \frac{-\alpha}{3} \cdot \frac{P_{es}}{EJT} \cdot (E_{es} - E_{ad}) \cdot \frac{1}{[E(t)]^{4/3}} \cdot \left(\frac{1}{P_{es} + V_0 \cdot E(t)}\right)^{2/3}. \tag{A9}$$

Peak shortening velocity of LV longitudinal length, S_m, corresponds to the absolute value of peak negative dL(*t*)/dt during the ejection phase. Because E(*t*) increases constantly during this period (Figure 1B), dL(*t*)/dt assumes its peak negative value when E(*t*) is E_{ad}. Hence, S_m can be expressed as follows:

$$S_m = \frac{\alpha}{3} \cdot \frac{P_{es}}{EJT} \cdot (E_{es} - E_{ad}) \cdot \frac{1}{E_{ad}^{4/3}} \cdot \left(\frac{1}{P_{es} + V_0 \cdot E_{ad}}\right)^{2/3}. \tag{A10}$$

As shown in Figure 1A, E_{es}, E_{ad}, and E_a will be approximated by P_{es}, V_{es}, V_{ed}, and V_0 as follows:

$$E_{es} = \frac{P_{es}}{V_{es} - V_0}; \tag{A11}$$

$$E_{ad} = \frac{P_{es}}{V_{ed} - V_0}, \tag{A12}$$

$$E_a = \frac{P_{es}}{V_{ed} - V_{es}}. \tag{A13}$$

Substituting V_{es} in equation A11 and V_{ed} in equation A12 into equation A13 yields

$$E_{es} - E_{ad} = \frac{E_{es} \cdot E_{ad}}{E_a}. \tag{A14}$$

Substituting $(E_{es} - E_{ad})$ in equation A14 into equation A10 yields

$$S_m = \frac{\alpha}{3} \cdot \frac{P_{es}}{EJT} \cdot \frac{E_{es}}{E_a} \cdot \frac{1}{E_{ad}^{1/3}} \cdot \left(\frac{1}{P_{es} + V_0 \cdot E_{ad}}\right)^{2/3}. \tag{A15}$$

Substituting E_{ad} in equation A12 into equation A15 yields

$$S_m = \frac{\alpha}{3} \cdot \frac{E_{es}}{E_a} \cdot \frac{V_{ed}^{1/3}}{EJT} \cdot \left(1 - \frac{V_0}{V_{ed}}\right). \tag{A16}$$

If we assume that $V_{ed} \gg V_0$, equation A16 is rewritten as

$$S_m = \frac{\alpha}{3} \cdot \frac{E_{es}}{E_a} \cdot \frac{V_{ed}^{1/3}}{EJT},$$

which is equation 1 shown in the "Methods" section.

Am J Physiol Regul Integr Comp Physiol 300: R818–R826, 2011.
First published February 2, 2011; doi:10.1152/ajpregu.00426.2010.

Imbalance of central nitric oxide and reactive oxygen species in the regulation of sympathetic activity and neural mechanisms of hypertension

Yoshitaka Hirooka, Takuya Kishi, Koji Sakai, Akira Takeshita,† and Kenji Sunagawa

Department of Cardiovascular Medicine, Kyushu University Graduate School of Medical Sciences, Fukuoka, Japan

Submitted 29 June 2010; accepted in final form 29 January 2011

Hirooka Y, Kishi T, Sakai K, Takeshita A, Sunagawa K. Imbalance of central nitric oxide and reactive oxygen species in the regulation of sympathetic activity and neural mechanisms of hypertension. *Am J Physiol Regul Integr Comp Physiol* 300: R818–R826, 2011. First published February 2, 2011; doi:10.1152/ajpregu.00426.2010.— Nitric oxide (NO) and reactive oxygen species (ROS) play important roles in blood pressure regulation via the modulation of the autonomic nervous system, particularly in the central nervous system (CNS). In general, accumulating evidence suggests that NO inhibits, but ROS activates, the sympathetic nervous system. NO and ROS, however, interact with each other. Our consecutive studies and those of others strongly indicate that an imbalance between NO bioavailability and ROS generation in the CNS, including the brain stem, activates the sympathetic nervous system, and this mechanism is involved in the pathogenesis of neurogenic aspects of hypertension. In this review, we focus on the role of NO and ROS in the regulation of the sympathetic nervous system within the brain stem and subsequent cardiovascular control. Multiple mechanisms are proposed, including modulation of neurotransmitter release, inhibition of receptors, and alterations of intracellular signaling pathways. Together, the evidence indicates that an imbalance of NO and ROS in the CNS plays a pivotal role in the pathogenesis of hypertension.

blood pressure; sympathetic nervous system; central nervous system; nitric oxide; oxidative stress

ACTIVATION OF THE SYMPATHETIC nervous system is critically involved in the pathogenesis of hypertension, from initial occurrence to the development of target organ damage, such as heart failure, stroke, and renal failure (35, 36). The importance of the effects of the renin-angiotensin system on the sympathetic nervous system in the pathogenesis of hypertension is recently highlighted (30, 31). This is not surprising because both the autonomic nervous system and hormonal factors are the major regulators of blood pressure; therefore, abnormalities of either system are likely to be involved in the pathogenesis of essential hypertension (30, 31, 37). Esler (30) reported that the sympathetic nervous system is activated in ~50% of patients with hypertension, particularly in patients with essential hypertension. Central sympathetic outflow is determined by several important nuclei and their circuits in the central nervous system (CNS) (9, 81). These pathways involve many neurotransmitters and neuromodulators (16, 25, 38, 99). In particular, the brain stem circuitry is now considered crucial for the pathogenesis of hypertension, including both excitatory and inhibitory inputs from the supramedullary nuclei and the baroreceptors (16, 25, 38, 100, 115). In this review, we focus on the role of nitric oxide (NO) and reactive oxygen species (ROS) in the brain stem as factors constituting the neural mechanisms of hypertension. Because of the close relationship between NO and ROS, we discuss the individual roles of NO and ROS in the brain stem in central mechanisms of hypertension, and then the relationship between the two. Finally, we will discuss the possibility of targeting some cardiovascular drugs to improve the imbalance of NO and ROS.

NO in the Brain

NO is an important mediator of intracellular signaling in various tissues, including the CNS (32, 118, 119). NO acts via the second messenger cyclic GMP (32). Thus, soluble guanylate cyclase is its receptor. NO is synthesized from its precursor, L-arginine, by endogenous NO synthase (NOS). There are three NOS isoforms: constitutive enzymes, such as neuronal NOS (nNOS) and endothelial NOS (eNOS), and inducible enzymes such as inducible NOS (iNOS). A number of studies have demonstrated the localization of the nNOS, eNOS, and iNOS within the CNS using in situ hybridization and histochemical staining with NADPH-diaphorase or immunohistochemistry (8). nNOS is abundant in neurons. Considerable evidence indicates that NOS acts on central and peripheral sites throughout the autonomic nervous system, which controls the cardiovascular system, including the receptors and effectors of the baroreflex pathway (70, 95, 129).

Role of NO in the Brain Stem in Controlling Blood Pressure

Chronic administration of the NO synthesis inhibitor N^{ω}-nitro-L-arginine methyl ester (L-NAME) in drinking water induces a large increase in blood pressure in rats (29). Gangli-

† Deceased March 15, 2009.

Address for reprint requests and other correspondence: Y. Hirooka, Dept. of Cardiovascular Medicine, Kyushu Univ., Graduate School of Medical Sciences, 3-1-1 Maidashi, Higashi-ku, Fukuoka 812-8582, Japan (e-mail: hyoshi@cardiol.med.kyushu-u.ac.jp).

onic blockade elicits a greater fall in blood pressure in L-NAME-treated rats compared with controls, suggesting that the level of central sympathetic outflow in L-NAME-treated rats is greater than that in control rats. Microinjection of an ANG II type 1 (AT_1) receptor blocker (candesartan), but not that of an AT_2 receptor blocker (PD123319), into the nucleus tractus solitarius (NTS) elicits a greater decrease in blood pressure, heart rate, and renal sympathetic nerve activity (RSNA) in L-NAME-treated rats than in control rats. These results suggest that increased RSNA contributes to hypertension induced by chronic NOS inhibition and that activation of the renin-angiotensin system in the NTS is involved, at least in part, in the increased RSNA via AT_1 receptors (29). The rostral ventrolateral medulla (RVLM), the vasomotor center, is also activated in this model of hypertension, suggesting enhanced central sympathetic outflow (9). Pharmacological inhibition of NOS evoked by N^G-monomethyl-L-arginine (L-NMMA) or L-NAME also induces large increases in blood pressure that are partially sympathetically mediated in humans (109).

Immunohistochemical studies have revealed a rich distribution of nNOS in the NTS (8). Microinjection of L-NMMA into the NTS elicits an increase in blood pressure and RSNA, regardless of whether the baroreceptors are intact in anesthetized rabbits (39). The neurons in the NTS are activated by NO projecting to the caudal ventrolateral medulla, thereby activating the inhibitory neurons in the caudal ventrolateral medulla, which project to the RVLM, and may ultimately result in decreased sympathetic nerve activity (SNA). Single-unit extracellular recordings of NTS neurons in rat brain stem slices revealed that L-arginine increases neuronal activity dose-dependently, but D-arginine does not (80, 116). L-NMMA blocks the L-arginine-induced increases in the neuronal activity. Sodium nitroprusside, an NO donor, also increases neuronal activity. Consistent with the findings from the in vivo studies (39), these results suggest that NO increases the neuronal activity in the NTS through an increase in cyclic GMP. It has been proposed that NO acts in an ultrashort feedback loop, in which the release of L-glutamate activates nNOS and subsequently the production of NO (32). The NO, in turn, diffuses to presynaptic terminals, where it modulates the release of L-glutamate in response to neuronal activation. Studies using in vivo microdialysis demonstrated that activation of NMDA receptors in the NTS induces the release of NO, and NMDA-induced NO production stimulates L-glutamate release (74, 75, 82). In addition, this mechanism is involved in the depressor and bradycardic responses evoked by NMDA receptor activation in anesthetized rats (82). To determine the effects of increased NO production in the NTS for much longer periods on blood pressure, heart rate, and urinary norepinephrine excretion, we developed an in vivo technique for eNOS gene transfer into the NTS of rats (43, 44, 46, 107). In this study, the successful transfer of the eNOS gene into the NTS was confirmed by several methods, including immunohistochemistry, Western blot analysis, and nitrite/nitrate concentration measurements (107). Changes in blood pressure and heart rate were observed using a radio-telemetry system. It is important to note that we used eNOS instead of nNOS, which is normally abundant in the CNS, because the purpose of the study was to increase NO production from constitutively expressed NOS. The results indicated that NO in the NTS exerts an inhibitory effect on SNA in vivo.

Compared to studies of the NTS, studies of the RVLM in both acute and anesthetized models have produced more conflicting results (42, 53, 66, 81, 112, 120, 131). Therefore, we applied the technique described above to studies of the RVLM (57, 58). In those studies, blood pressure, heart rate, and urinary norepinephrine excretion were decreased after eNOS gene transfer. Microinjection of either L-NMMA or bicuculine, a GABA receptor antagonist, into the RVLM after eNOS gene transfer increased blood pressure to greater levels in the eNOS gene transfer group compared with the mock gene transfer control group. GABA levels in the RVLM after the eNOS gene transfer measured by in vivo microdialysis were also increased in the eNOS gene transfer group. These results indicate that the increased NO production evoked by the overexpression of eNOS in the bilateral RVLM decreases blood pressure, heart rate, and SNA in awake rats. Furthermore, these responses are mediated by an increased release of GABA in the RVLM. These studies provided convincing evidence that chronic changes in neurotransmitters/neuromodulators in the RVLM have a sustained impact on blood pressure in awake animals.

There is no clear explanation for the different modulatory effects of NO on neurons between the NTS and RVLM. NO increases both excitatory and inhibitory amino acids in the RVLM (43, 57). NO has also been shown to increase both L-glutamate and GABA in the paraventricular nucleus of hypothalamus (49). Microinjection of kynurenic acid into the RVLM, however, did not alter blood pressure after eNOS gene transfer, although microinjection of bicuculline into the RVLM augmented the increase in blood pressure (57). Therefore, we consider that GABAergic inhibition of the RVLM neurons might be more powerful than the glutamatergic activation in the resting condition (43, 57). In contrast, the glutamatergic input into the NTS neurons might be more powerful than the GABAergic input. In the NTS, there are close anatomic connections between nNOS and glutamatergic receptors (75). Furthermore, increases in NO induce L-glutamate release and microinfusion of NMDA and AMPA increase NO levels, suggesting that there are facilitatory interactions between L-glutamate and NO (27, 74, 82), although there are no studies measuring GABA levels induced by NO in the NTS. Furthermore, higher concentrations of NO are required to directly engage GABAergic inhibition, while lower concentrations of NO might be important for glutamatergic transmission in the NTS (125). Thus, it is still difficult and complicated to explain the physiological response induced by NO in the NTS (119). With regard to the action of NO on neuronal activity, NO induces both excitatory and inhibitory postsynaptic currents that likely depend on the neuron examined (6, 7, 126, 127).

Effects of NO in the Brain System in Experimental Models of Hypertension

Neurogenic mechanisms are dominant in the pathogenesis of essential hypertension in ~50% of patients (30). Spontaneously hypertensive rats (SHR) or stroke-prone SHR (SHRSP) exhibit increased RSNA during the development of hypertension, and blood pressure and RSNA are positively correlated (52, 79). The L-arginine-NO pathway is disrupted in SHR and SHRSP. The depressor response to an intracerebroventricular injection of an NO donor is greater in SHRSP than in normo-

tensive control rats, whereas the pressor response to intracerebroventricular injection of L-NAME is smaller (13). Semiquantitative RT-PCRs and in situ hybridization in SHR and Wistar-Kyoto (WKY) rats at 4 (prehypertensive) and 14 (established hypertension) wk of age (101) indicate that eNOS mRNA expression changes with the development of hypertension. Although there are no differences between the groups at 4 wk of age, nNOS gene expression increases in the hypothalamus, dorsal medulla, and caudal ventrolateral medulla of SHR compared with WKY rats at 14 wk of age. In the RVLM, there are no differences between the groups. In the SHRSP, there are also no differences in nNOS expression levels in the RVLM compared with WKY rats (101). A recent study demonstrated that NOS activity, measured by the ability of tissue homogenate to convert [^{3}H]L-arginine to [^{3}H]L-citrulline in a calcium- and NADPH-dependent manner, is impaired in the cerebral cortex and brain stem of prehypertensive SHR (104). In contrast, NOS activity is increased in the hypothalamus and brain stem in SHR rats with established hypertension compared with WKY rats (104). Thus, attenuated NOS activity in the cortex and brain stem of prehypertensive SHR might play a role in the pathogenesis of hypertension, and the up-regulated NOS activity in the hypothalamus and brain stem of SHR with established hypertension might serve to compensate for the hypertension. The expression of iNOS mRNA and protein is under the limits of detection in the hypothalamus of both WKY rats and SHR (40). Decreased NOS activity measured by the nitrite and nitrate contents was also demonstrated in the hypothalamus of SHR (1). In hypertensive SHRSP, nNOS protein expression levels in the hypothalamus and brain stem were enhanced compared with those in WKY (59). In a renovascular hypertensive rat model, mRNA expression levels of nNOS and soluble guanylate cyclase genes are reduced in the hypothalamus but not in the dorsal medulla (69). Together, these results suggest that the L-arginine-NO pathway is impaired in hypertensive rats, including SHR, possibly because of a posttranscriptional abnormality (70). Overexpression of eNOS in the NTS results in a greater depressor response in SHR than in WKY rats in the awake state (44). In that study, eNOS was used instead of nNOS to increase NO production locally in the NTS. Findings from another study suggest that the depressed NO modulation is consistent with the lower NOS activity in the dorsal brain stem (103). Therefore, the abnormality in the L-arginine-NO pathway in the NTS might be involved in the maintenance of hypertension of SHR. A recent study by Waki et al. (121) demonstrated that endogenous eNOS activity in the NTS plays a major role in determining the blood pressure set point in SHR and contributes to maintaining high arterial blood pressure in this model, suggesting the possible involvement of neurovascular coupling (96). In the RVLM of SHRSP, overexpression of eNOS elicits greater depressor and sympathoinhibitory responses than in WKY (58). Furthermore, the increase in NO production evoked by the overexpression of eNOS in the RVLM enhances the inhibitory action of GABA on the RVLM neurons (58). The results indicate that NO dysfunction and the resulting disinhibition of the RVLM contribute to increase RSNA in SHRSP.

Effects of NO in the Brain Stem on Baroreflex Function

As described earlier, NO activity in the NTS and RVLM influences cardiovascular regulation. We examined the role of endogenous NO in the brain stem in the rapid central adaptation of baroreflex control of RSNA in anesthetized rabbits (41). Bilateral carotid sinuses were isolated, and a stepwise increase in pressure was applied to the carotid sinuses, while arterial pressure and RSNA were recorded. The procedure was performed after intracisternal injection of L-NAME, D-NAME, L-arginine, or the vehicle solution. L-NAME enhances the rapid adaptation of the arterial baroreflex control of renal sympathetic nerve activity in rabbits (41). Transmission of arterial baroreflex signals depends on NO (27, 118). It was reported that the baroreceptor reflex gain in awake animals was increased by NO in the bradycardic component, although in these studies NOS inhibitors were administered systemically to examine the role of NO on baroreflex function (78, 87). Furthermore, overexpression of eNOS in the RVLM improves impaired baroreflex control of heart rate in SHRSP (60).

In summary, NO in the brain stem, particularly in the NTS and RVLM, has a sympathoinhibitory function, thereby reducing blood pressure. NO in the brain stem also facilitates the baroreflex function. The sympathoinhibitory effects of NO are impaired in animal models of hypertension, and supplementation of NO in the brain stem in hypertensive rats attenuates the abnormality, thereby decreasing blood pressure. The facilitory release of neurotransmitters induced by NO might be involved in the synaptic transmission mechanism.

ROS in the Brain

Substantial evidence also indicates that increased oxidative stress is involved in the pathogenesis of hypertension (12, 47, 48, 94, 99). ROS, such as superoxide anions and hydroxyl radicals, increase oxidative stress. There are several sources of ROS generation, such as NADPH oxidase, xanthine oxidase, mitochondria, and NOS uncoupling (12, 47, 48, 94, 99). On the other hand, reduction of antioxidant enzymes, such as superoxide dismutases (SOD), also induces an increase in oxidative stress (47, 48, 99). Although the role of ROS in the regulation of blood pressure in the normotensive state is not clear, increased ROS generation in the brain stem contributes to neural mechanisms of hypertension (47, 48). For example, although there is evidence of an increase in oxidative stress in the vasculature in hypertension, we showed, for the first time, that increased ROS in the RVLM contributes to SNA, leading to the neural mechanisms of hypertension in SHRSP (61). Zimmerman et al. (133) demonstrated that hypertension caused by low doses of circulating ANG II depends on the production of superoxide in the circumventricular organs (133). It was demonstrated that physiological responses to brain ANG II involve ROS production (15, 132, 133). Considering the importance of the brain ANG II system (2, 10, 26, 28, 83, 85, 86, 108), ROS play an important role in the neural regulation of blood pressure because ROS production largely depends on AT_1 receptor stimulation (47, 48, 99).

Role of ROS in Neural Mechanisms of Hypertension

As described earlier, on the basis of results demonstrating that microinjection of Tempol or overexpression of manga-

nese-superoxide dismutase in the RVLM markedly decreases blood pressure in SHRSP, but not in WKY, increased oxidative stress in the RVLM contributes to the neural mechanisms of hypertension in SHRSP (61). Oxidative stress levels in the RVLM were determined by measuring thiobarbituric acid-reactive substances (TBARS) levels and electron spin resonance (ESR) spectroscopy with a spin trapping technique (47, 48, 61). In SHR, oxidative stress in the RVLM plays an important role in hypertension via activation of the sympathetic nervous system (19, 66, 106, 117). An increase in oxidative stress in the RVLM also contributes to hypertension via activation of the sympathetic nervous system in rats with renovascular hypertension (two-kidney one-clip hypertensive model) (92). This model is an ANG II-dependent model of hypertension. Therefore, it is conceivable that ANG II increases oxidative stress by acting both centrally and peripherally, thereby activating the sympathetic nervous system and leading to hypertension as one of the hypertensive mechanisms in this model. AT_1 receptor expression levels in the RVLM and the paraventricular nucleus of the hypothalamus are enhanced in this rat renovascular model of hypertension (93). Interestingly, NADPH oxidase activity is increased, but Cu/Zn-SOD expression in the RVLM is unchanged. In a subsequent study, the authors showed that oxidative stress increased in both the RVLM and paraventricular nucleus, as well as systemically in this hypertensive model (93). These results suggest that systemic activation of the renin-angiotensin system activates AT_1 receptors in the brain, including the RVLM and paraventricular nucleus, thereby increasing SNA, leading to hypertension, as one of the mechanisms.

Sources of ROS Generation in the Brain Stem

NADPH oxidase is a major source of ROS in hypertension (71, 72) and has a critical role in generating ROS in the brain (5, 14, 51, 90, 122, 134). ANG II is upstream of NADPH oxidase activation, which requires Rac1 (48, 90, 122, 134). NADPH oxidase-derived ROS are involved in the effects of ANG II on Ca^{2+} influx in the NTS neurons receiving vagal afferents (122). Importantly, the essential subunit of NADPH oxidase, gp91phox, is present in somatodendritic and axonal profiles containing AT_1 receptors (122). The potentiation of Ca^{2+} currents indicates that ANG II increases neuronal excitability and spontaneous activity in some neurons (135). ANG II failed to increase ROS production or to potentiate L-type Ca^{2+} currents in the dorsomedial portion of the NTS neurons of mice lacking Nox2 (123). Thus, the excitatory actions of ANG II in the NTS neurons are caused, at least, in part, by the activation of L-type Ca^{2+} channels. It should be noted that ANG II-induced inhibition of neuronal delayed rectifying potassium current (I_{KV}) is mediated by ROS in primary neurons isolated from the hypothalamus and brain stem, because both NAD(P)H oxidase inhibition and Tempol prevented the ANG II inhibition of I_{KV} (113).

Mitochondria are another source of ROS generation in the brain. Chan et al. (21) examined the role of the mitochondrial electron transport chain in the RVLM of SHR and found that mitochondrial electron transport chain dysfunction in the RVLM of SHR depressed complex I or III activity and reduced the electron transport capacity (ETC) between complexes I and III or II and III (21). Interestingly, microinjection of coenzyme Q_{10} into the RVLM of SHR reversed the depressed ETC activity and enhanced superoxide generation. In addition, microinjection of antisense oligonucleotide against the p22phox subunit of NADPH oxidase into the RVLM reduced the enhanced ROS production in SHR (21). It is also important to note that microinjection of coenzyme Q_{10} into the RVLM of SHR decreases blood pressure (21). These results suggest that impairment of mitochondrial ETC complexes contributes to chronic oxidative stress in the RVLM of SHR, leading to enhanced central sympathetic drive and hypertension (21, 136). Consistent with their observation, we also found that ANG II induced the mitochondria-derived ROS production via activation of NADPH oxidase, although we did not find differences in the mitochondrial respiratory complexes between SHRSP and WKY (91), thus suggesting a feedforward system for ROS generation (21, 91, 136) (Fig. 1). Mitochondrial produced superoxide mediates the ANG II inhibition of I_{KV} (128). Recently, Chan et al. (22) suggested that transcriptional upregulation of mitochondrial uncoupling protein 2 (UCP2) in response to an increase in superoxide plays an active role in the feedback regulation of ROS production in the RVLM (22). Furthermore, oral treatment with rosiglitazone enhances a central antihypertensive effect via an upregulation of peroxisome proliferator-activated receptor-γ (PPAR-γ) and reduced oxidative stress in the RVLM of SHR (23). Stimulation of PPAR-γ results in the upregulation of UCP2, thereby reducing oxidative stress. The dose of rosiglitazone used in that study,

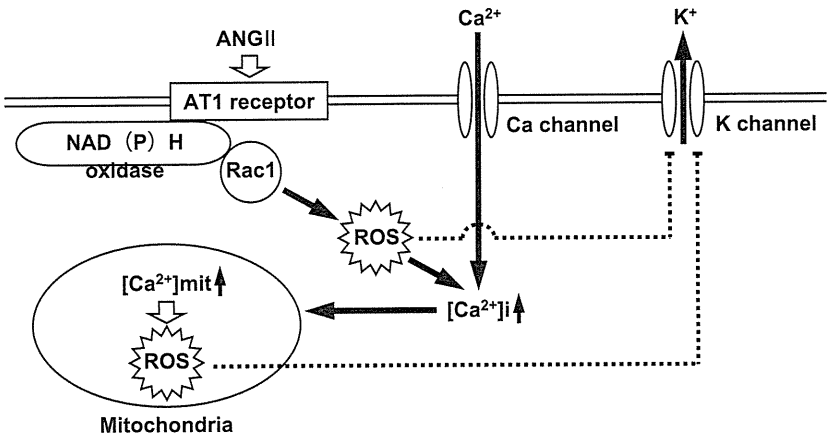

Fig. 1. A suggested scheme demonstrating that ANG II stimulation increases reactive oxygen species (ROS) generation via NAD(P)H oxidase and related mechanisms. [Modified from Nozoe et al. (91).]

however, was fairly high, and this does not necessarily relate to the clinical setting.

Downstream Signaling Pathway of the AT_1 Receptor Stimulation in the RVLM Involving ROS Production

As described above, activation of the AT_1 receptor produces superoxide anions as an initial step of ROS generation through NADPH oxidase. Thus, the signaling pathway should be pivotal for neuronal activation leading to hypertension via central sympathetic outflow. NAD(P)H oxidase-derived ROS production mediates the ANG II-induced pressor response via activation of p38 MAPK and ERK in the RVLM (18, 20). Chan et al. (20) demonstrated that intracerebroventricular infusion of ANG II elicits the long-term pressor response, and this pressor response is mediated by protein kinase C/ERK/cyclic adenosine monophosphate response element binding protein and c-*fos* induction (20). It should be noted that the ANG II-induced pressor response might not necessarily be related to ROS production in the RVLM. The ANG II-induced pressor response, however, is significantly inhibited by ROS scavenging, and endogenous blockade of AT_1 receptors in the brain stem of SHRSP reduces ROS and blood pressure (48, 91). Activation of caspase-3 acting through the Ras/p38 MAPK/ERK pathway in the RVLM might be involved in sympathoexcitation of SHRSP (65). In addition, the apoptotic proteins Bax and Bad are activated, and the antiapoptotic protein Bcl-2 is inhibited in the RVLM of SHRSP (65). The Ras inhibitor substantially attenuated these changes, thereby attenuating caspase-3 associated with the decrease in blood pressure. In contrast, however, c-Jun N-terminal kinase activity was not altered in the RVLM of SHRSP compared with that of WKY (65). It should be noted that the possibility of caspase-3-independent neuronal apoptosis in the RVLM or of a direct link between ROS and caspase-3 activation was not examined in that study (65). However, this finding is consistent with the results demonstrating that microinjection of ANG II induces AT_1 receptor-dependent ROS production and phosphorylation of p38 MAPK and ERK, but not stress-activated protein kinase/Jun N-terminal kinase in the RVLM of Sprague-Dawley rats (18). Interestingly, this is not the case in the RVLM of heart failure rabbits (77). Stress-activated protein kinase/Jun N-terminal kinase activity was increased in the RVLM of these heart failure rabbits (77). The increased phosphorylation of Jun N-terminal kinase may lead to activation of the transcription factor AP-1, which is a dimer of Jun and c-Fos family members. It is not clear why these differences between hypertension and heart failure occur. It is possible that signal transduction changes in the progression from hypertension to heart failure, thereby leading to further enhanced central sympathetic outflow. Further studies are needed to establish a more direct link between these signaling pathways, redox sensitivity, and the development and/or progression of hypertension.

Imbalance of Brain NO and ROS

Superoxide derived from NADPH oxidase reacts with and inactivates NO and thereby modulates its bioavailability (32, 97, 114) (Fig. 2). The converse is also true; that is, NO reduces superoxide, which may be beneficial (32, 99) (Fig. 2). An increase in NO in the RVLM decreases blood pressure and sympathetic nervous system activity to a greater extent in

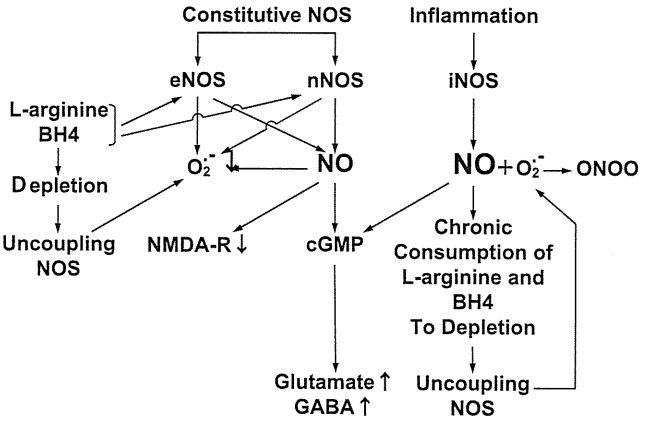

Fig. 2. A scheme demonstrating the interaction between nitric oxide (NO) and ROS generation. NMDA-R, *N*-methyl-D-aspartate receptors; GABA, γ-aminobutyric acid; BH4, tetrahydrobiopterin; NOS, nitric oxide synthase; eNOS, endothelial NOS; iNOS, inducible NOS; nNOS, neuronal NOS. [Modified from Hirooka (47).]

SHRSP than in WKY rats (58). This might be due to a reduction in superoxide via NO in the RVLM of SHRSP, which is increased in the RVLM of SHRSP (61). All three NOS isoforms generate superoxide depending on substrate (L-arginine) and cofactor (tetrahydrobiopterin) availability (32, 97, 114). The induction of both iNOS and ROS during inflammation is well established (88, 97). A recent study suggested that ROS and reactive nitrogen species, such as peroxynitrite dose-dependently regulate iNOS function (114). Overexpression of iNOS in the RVLM causes sympathoexcitation via an increase in oxidative stress (54). As expected, the release of more nitrite/nitrate (NO_x) in RVLM dialysate is induced by iNOS overexpression than by eNOS overexpression (54). Relative to the constitutive isoforms, iNOS has approximately five-fold higher NO production (97). NO_x release, however, is increased by approximately twofold higher by iNOS overexpression than by eNOS overexpression (54). We considered that the precursor of NO production, L-arginine, and its cofactor, tetrahydrobiopterin, might be consumed and insufficient when iNOS is chronically expressed, thereby iNOS would produce superoxide instead of NO (Fig. 2). Otherwise, chronic overexpression of iNOS increases levels of NO chronically, which, in turn, reacts with superoxide in a diffusion-limited reaction to produce peroxinitrite (Fig. 2). In fact, we found an increase in the TBARS levels in the RVLM and the pressor response after overexpression of iNOS. The increased pressor response was, however, abolished by iNOS inhibitors or Tempol. Once ROS production is increased, ROS enhance superoxide production from iNOS, indicating that ROS promote iNOS uncoupling. Further, peroxynitrite, produced from the reaction between NO and superoxide, reduces both NO and superoxide generation, indicating that peroxynitrite causes iNOS dysfunction enzymatically. In our study, we detected some iNOS-positive cells with the antinitrotyrosine antibody (54). Furthermore, iNOS expression levels were increased in the RVLM of SHRSP compared with WKY (56). Kung et al. (68) suggested that mitochondrial respiratory enzyme complexes in the RVLM were cellular targets of NO and ROS interaction after eNOS gene transfer. This concept is problematic, however, in that they suggest that superoxide and per-

oxynitrite are produced after eNOS gene transfer into the RVLM (68). Another recent study suggested that NMDA receptor activation increases ROS production through NO and Nox2 (33). Further studies are needed to explore whether this mechanism functions via ubiquitous glutamatergic synaptic transmission in vivo.

Sympathoinhibitory Effects of Antihypertensive Drugs and Statins

NADPH oxidase, which is activated by AT_1 receptor stimulation, is a major source of ROS (11, 17, 113, 135). The specific brain nuclei that regulate SNA, such as the anteroventral third ventricle, paraventricular nucleus of the hypothalamus, NTS, and the RVLM, are rich in AT_1 receptors (2, 10, 26, 28, 83). AT_1 receptor expression levels are upregulated in the RVLM of hypertensive animal models compared with normotensive controls (105). Thus, it is possible that AT_1 receptor blockers reduce oxidative stress in the brain, as well as in the peripheral vasculature. It is also possible that AT_1 receptor blockers inhibit ROS production by blocking AT1 receptor-mediated intracellular signaling (11, 48, 50) and that this antioxidant action accounts for the absence of reflex-induced sympathoexcitation after treatment with AT_1 receptor blockers. We evaluated the effects of AT_1 receptor blockers, olmesartan and telmisartan, on brain oxidative stress in SHRSP (4, 48). Both AT_1 receptor blockers have antioxidant properties in the brain without stimulating reflex-mediated SNA in SHRSP. We used in vivo ESR spectroscopy to examine the effect of oral olmesartan on oxidative stress in the brain (4), because the in vivo ESR method is a powerful technique for evaluating oxidative stress (3, 110, 111). The effects of peripherally administered olmesartan or telmisartan on central sympathetic outflow have been demonstrated in other studies (34, 76). Are these antioxidant effects of olmesartan or telmisartan specific for each drug or the AT_1 receptor blocker class? Other angiotensin receptor blockers, such as losartan or candesartan, have similar sympatho-inhibitory effects in the CNS, although there are some differences among angiotensin receptor blockers (24, 89, 102, 124). The differences of the central effects of each angiotensin receptor blocker might depend on its lipophilicity, phamacokinetics, and the transporter system (24, 34, 48, 124). Furthermore, systemically administered candesartan reduces brain ANG II via downregulation of the brain renin-angiotensin system (98). This finding provides new mechanistic insight into the treatment of hypertension by the AT_1 receptor blockers (84). Unfortunately, however, these effects of AT_1 receptor blockers, that is, reduction of brain oxidative stress and sympatho-inhibitory effects, even when administered systemically, are usually ignored by researchers or clinicians, but should be considered as potential therapeutic candidates.

Considering the inhibitory effects of AT_1 receptor blockers on brain oxidative stress and sympathetic nervous system activity, it would be interesting to know whether other cardiovascular drugs have similar effects. We found that atorvastatin causes depressor and sympathoinhibitory effects with upregulation of NOS in SHRSP (59), which is consistent with the effects of statins on eNOS upregulation in the vasculature (55). Atorvastatin also reduces oxidative stress in the RVLM of SHRSP (62, 63, 64). With regard to the central sympathoinhibitory effects of calcium channel blockers, lipophilic dihydropyridine calcium channel blockers, such as nifedipine, nisoldipine, and amlodipine, readily cross the blood-brain barrier, thereby presumably blocking brain L-type Ca^{2+} channels leading to central sympathoinhibition (73). It is generally considered that an arterial baroreflex-mediated increase in sympathetic activity is responsible for the unfavorable effects of short- and strong-acting dihydropyridine calcium channel blockers; therefore, the intrinsic sympathoinhibitory effects of calcium channel blockers have been ignored. These findings together suggest that increased NOS activity and antioxidant effects in the brain stem might be involved in the central sympathoinhibitory effects of some calcium channel blockers (45, 55, 67). The precise mechanisms involved, however, remain unknown, and further studies are required.

Summary and Conclusions

In summary, accumulating evidence indicates that an imbalance of NO and ROS in the CNS, particularly in the brain stem, is crucially involved in hypertension via the activation of central sympathetic outflow. Upstream and downstream consequences of the precise mechanisms are discussed. Several questions remain, however, because the interactions between NO and ROS are complex. Further studies are required to gain a better understanding of the role of brain NO and ROS in autonomic cardiovascular regulation and potential therapeutic targets.

GRANTS

This series of studies was supported by the Grants-in Aid for Scientific Research from the Japan Society for Promotion of Science and, in part, by a Grant from Kimura Memorial Foundation Research.

DISCLOSURES

No conflicts of interest, financial or otherwise, are declared by the authors.

REFERENCES

1. **Alaghband-Zadeh J, Das I, Hanson MR, MacGregor CAL, de Wardener HE, Laycock JF.** Hypothalamic and plasma total nitrate/nitrite concentrations in spontaneously hypertensive rats. *Exp Physiol* 81: 881–883, 1996.
2. **Allen AM, O'Callaghan EL, Chen D, Bassi JK.** Central neural regulation of cardiovascular function by angiotensin: a focus on the rostral ventrolateral medulla. *Neuroendocrinology* 89: 361–369, 2009.
3. **Anzai K, Saito K, Takeshita K, Takahashi S, Miyazaki H, Shoji H, Lee MC, Masumizu T, Ozawa T.** Assessment of ESR-CT imaging by comparison with autoradiography for the distribution of a blood-brain-barrier permeable spin probe, MC-PROXYL, to rodent brain. *Magn Reson Imaging* 21: 765–772, 2003.
4. **Araki S, Hirooka Y, Kishi T, Yasukawa K, Utsumi H, Sunagawa K.** Olmesartan reduces oxidative stress in the brain of stroke-prone spontaneously hypertensive rats assessed by an in vivo ESR method. *Hypertens Res* 32: 1091–1096, 2009.
5. **Bai Y, Jabbari B, Ye S, Campese VM.** Regional expression of NAD(P)H oxidase and superoxide dismutase in the brain of rats with neurogenic hypertension. *Am J Nephrol* 29: 483–492, 2009.
6. **Bains JS, Ferguson AV.** Nitric oxide depolarizes type II paraventricular nucleus neurons in vitro. *Neuroscience* 79: 149–159, 1997.
7. **Bains JS, Ferguson AV.** Nitric oxide regulates NMDA-drived GABAergic inputs to type I neurons of the rat paraventricular nucleus. *J Physiol* 499: 733–746, 1997.
8. **Batten TFC, Atkinson L, Deuchars J.** Nitric oxide systems in the medulla oblongata and their involvement in autonomic control. In: *Functional Neuroanatomy of the Nitric Oxide System. Handbook of Chemical Neuroanatomy*, edited by Steinbusch HWM, De Vente J, Vincent SR, Amsterdam, The Netherlands: Elsevier, 177–213, 2000.

9. **Bergamaschi CT, Campos RR, Lopes OU.** Rostral ventrolateral medulla: a source of sympathetic activation in rats subjected to long-term treatment with L-NAME. *Hypertension* 34: 744–747, 1999.
10. **Bourassa EA, Sved AF, Speth RC.** Angiotensin modulation of rostral ventrolateral medulla (RVLM) in cardiovascular regulation. *Mol Cell Endocrinol* 302: 167–175, 2009.
11. **Brandes RP.** Vascular functions of NADPH oxidases. *Hypertension* 56: 17–21, 2010.
12. **Briones AM, Touyz RM.** Oxidative stress and hypertension: current concepts. *Curr Hypertens Rep* 12: 135–142, 2010.
13. **Cabrena CL, Bealer SL, Bohr DF.** Central depressor action of nitric oxide is deficient in genetic hypertension. *Am J Hypertens* 9: 237–241, 1996.
14. **Campese VM, Sindhu RK, Ye S, Bai Y, Vaziri ND, Jabbari B.** Regional expression of NO synthase, NAD(P)H oxidase and superoxide dismutase in the rat brain. *Brain Res* 1134: 27–32, 2007.
15. **Campese VM, Shaohua Y, Huiquin Z.** Oxidative stress mediates angiotensin II-dependent stimulation of sympathetic nerve activity. *Hypertension* 46: 533–539, 2005.
16. **Campos RR, Bergamaschi CT.** Neurotransmission alterations in central cardiovascular control in experimental hypertension. *Curr Hypertens Rev* 2: 193–198, 2006.
17. **Campos RR.** Oxidative stress in the brain and arterial hypertension. *Hypertens Res* 32: 1047–1048, 2009.
18. **Chan SHH, Hsu KS, Huang CC, Wang LL, Ou CC, Chan JYH.** NADPH oxidase-derived superoxide anion mediates angiotensin II-induced pressor effect via activation of p38 mitogen-activated protein kinase in the rostral ventrolateral medulla. *Circ Res* 97: 772–780, 2005.
19. **Chan SHH, Tai MH, Li CY, Chan JYH.** Reduction in molecular synthesis or enzyme activity of superoxide dismutase and catalase contributes to oxidative stress and neurogenic hypertension in spontaneously hypertensive rats. *Free Radic Biol Med* 40: 2028–2039, 2006.
20. **Chan SHH, Wang LL, Tseng HL, Chan JYH.** Upregulation of AT_1 receptor gene on activation of protein kinase Cβ/nicotinamide adenine dinucleotide diphosphate oxidase/ERK1/2/c-*fos* signaling cascade mediates long-term pressor effect of angiotensin II in rostral ventrolateral medulla. *J Hypertens* 25: 1845–1861, 2007.
21. **Chan SHH, Wu KLH, Chang AYW, Tai MH, Chan JYH.** Oxidative impairment of mitochondrial electron transport chain complexes in rostral ventrolateral medulla contributes to neurogenic hypertension. *Hypertension* 53: 217–227, 2009.
22. **Chan SHH, Wu CA, Wu KLH, Ho YH, Chang AYW, Chang JYH.** Transcriptional upregulation of mitochondrial uncoupling protein 2 protects against oxidative stress-associated neurogenic hypertension. *Circ Res* 105: 886–896, 2009.
23. **Chan SHH, Wu KLH, Kung PSS, Chan JYH.** Oral intake of rosiglitazone promotes a central antihypertensive effect via upregulation of peroxisome proliferator-activated receptor- and alleviation of oxidative stress in rostral ventrolateral medulla of spontaneously hypertensive rats. *Hypertension* 55: 1444–1453, 2010.
24. **Culman J, Blume A, Gohlke P, Unger T.** The renin-angiotensin system in the brain: possible therapeutic implications for AT_1-receptor blockers. *J Hum Hypertens* 16: S64–S70, 2002.
25. **Dampney RAL.** Functional organization of central pathways regulating the cardiovascular system. *Physiol Rev* 74: 323–364, 1994.
26. **Dampney RAL, Fontes MAP, Hirooka Y, Potts PD, Tagawa T.** Role of angiotensin II receptors in the regulation of vasomotor neurons in the rostral ventrolateral medulla. *Clin Exp Pharmacol Physiol* 29: 467–472, 2002.
27. **Dias AC, Vitela M, Colombari E, Mifflin SW.** Nitric oxide modulation of glutamatergic, baroreflex, and cardiopulmonary transmission in the nucleus of the solitary tract. *Am J Physiol Heart Circ Physiol* 288: H256–H262, 2005.
28. **Dupont AG, Brouwers S.** Brain angiotensin peptides regulate sympathetic tone and blood pressure. *J Hypertens* 28: 1599–1610, 2010.
29. **Eshima K, Hirooka Y, Shigematsu H, Matsuo I, Koike G, Sakai K, Takeshita A.** Angiotensin in the nucleus tractus solitarii contributes to neurogenic hypertension caused by chronic nitric oxide synthase inhibition. *Hypertension* 36: 259–263, 2000.
30. **Esler M.** Sympathetic nervous activation in essential hypertension: commonly neglected as a therapeutic target, usually ignored as a drug side effect. *Hypertension* 55: 1090–1091, 2010.
31. **Esler M.** The 2009 Carl Ludwig Lecture. Pathophysiology of the human sympathetic nervous system in cardiovascular diseases: the translation from mechanisms to medical management. *J Appl Physiol* 108: 227–237, 2010.
32. **Garthwaite J.** Concepts of neural nitric oxide-mediated transmission. *Eur J Neurosci* 27: 2783–2802, 2008.
33. **Girouard H, Wang G, Gallo EF, Anthrather J, Zhou P, Pickel VM, Iadecola C.** NMDA receptor activation increases free radical production through nitric oxide and Nox2. *J Neurosci* 29: 2545–2552, 2009.
34. **Gohlke P, Weiss S, Jansen A, Wienen W, Stangier J, Rascher W, Culman J, Unger T.** AT1 receptor antagonist telmisartan administered peripherally inhibits central responses to angiotensin II in conscious rats. *J Pharmacol Exp Ther* 298: 62–70, 2001.
35. **Grassi G.** Assessment of sympathetic cardiovascular drive in human hypertension: achievements and perspectives. *Hypertension* 54: 690–697, 2009.
36. **Grassi G.** Sympathetic neural activity in hypertension and related diseases. *Am J Hypertens* 23: 1052–1060, 2010.
37. **Grassi G, Seravalle G, Quarti-Trevano F.** The 'neurogenic hypothesis' in hypertension: current evidence. *Exp Physiol* 95: 581–586, 2010.
38. **Guyenet PG.** The sympathetic control of blood pressure. *Nat Rev Neurosci* 7: 335–346, 2006.
39. **Harada S, Tokunaga S, Momohara M, Masaki H, Tagawa T, Imaizumi T, Takeshita A.** Inhibition of nitric oxide formation in the nucleus tractus solitarius increases renal sympathetic nerve activity in rabbits. *Circ Res* 72: 511–516, 1993.
40. **Haüser W, Sassmann A, Qadri F, Jöhren O, Dominiak P.** Expression of nitric oxide synthase isoforms in hypothalamo-pitutary-adrenal axis during the development of spontaneously hypertension in rats. *Mol Brain Res* 138: 198–204, 2005.
41. **Hironaga K, Hirooka Y, Matsuo I, Shihara M, Tagawa T, Harasawa Y, Takeshita A.** Role of endogenous nitric oxide in the brain stem on the rapid adaptation of baroreflex. *Hypertension* 31: 27–31, 1998.
42. **Hirooka Y, Polson JW, Dampney RAL.** Pressor and sympathoexcitatory effects of nitric oxide in the rostral ventrolateral medulla. *J Hypertens* 14: 1317–1324, 1996.
43. **Hirooka Y, Kishi T, Sakai K, Shimokawa H, Takeshita A.** Effect of overproduction of nitric oxide in the brain stem on the cardiovascular response in conscious rats. *J Cardiovasc Pharmacol* 41 *Suppl* 1: S119–S126, 2003.
44. **Hirooka Y, Sakai K, Kishi T, Ito K, Shimokawa H, Takeshita A.** Enhanced depressor response to endothelial nitric oxide synthase gene transfer into the nucleus tractus solitarii of spontaneously hypertensive rats. *Hypertens Res* 26: 325–331, 2003.
45. **Hirooka Y, Kimura Y, Nozoe M, Sagara Y, Ito K, Sunagawa K.** Amlodipine-induced reduction of oxidative stress in the brain is associated with sympatho-inhibitory effects in stroke-prone spontaneously hypertensive rats. *Hypertens Res* 29: 49–56, 2006.
46. **Hirooka Y.** Localized gene transfer and its application for the study of central cardiovascular control. *Auton Neurosci* 126–127: 120–129, 2006.
47. **Hirooka Y.** Role of reactive oxygen species in brainstem in neural mechanisms of hypertension. *Auton Neurosci* 142: 20–24, 2008.
48. **Hirooka Y, Sagara Y, Kishi T, Sunagawa K.** Oxidative stress and central cardiovascular regulation: pathogenesis of hypertension and therapeutic aspects. *Circ J* 74: 827–835, 2010.
49. **Horn T, Smith PM, McLaughlin BE, Bauce L, Marks GS, Pittman QJ, Ferguson AV.** Nitric oxide actions in paraventricular nucleus: cardiovascular and neurochemical implications. *Am J Physiol Regul Integr Comp Physiol* 266: R306–R313, 1994.
50. **Inaba S, Iwai M, Furuno M, Tomono Y, Senba I, Okayama H, Mogi M, Higaki J, Horiuchi M.** Continuous activation of renin-angiotensin system impairs cognitive function in renin/angiotensinogen transgenic mice. *Hypertension* 53: 356–362, 2009.
51. **Infanger DW, Shrama RV, Davisson RL.** NADPH oxidases of the brain: distribution, regulation, and function. *Antioxid Redox Signal* 8: 1583–1596, 2006.
52. **Judy WV, Watanabe AM, Henry DP, Besch HR, Murphy WR, Hockel GM.** Sympathetic nerve activity: role in regulation of blood pressure in the spontaneously hypertensive rat. *Circ Res* 38: I-121–I-129, 1976.
53. **Kagiyama S, Tsuchihashi T, Abe I, Fujishima M.** Cardiovascular effects of nitric oxide in the rostral ventrolateral medulla of rats. *Brain Res* 757: 155–158, 1997.
54. **Kimura Y, Hirooka Y, Sagara Y, Ito K, Kishi T, Shimokawa H, Takeshita A, Sunagawa K.** Overexpression of inducible nitric oxide synthase in rostral ventrolateral medulla causes hypertension and sym-

pathoexcitation via an increase in oxidative stress. *Circ Res* 96: 252–260, 2005.
55. **Kimura Y, Hirooka Y, Sagara Y, Sunagawa K.** Long-acting calcium channel blocker, azelnidipine, increases endothelial nitric oxide synthase in the brain and inhibits sympathetic nerve activity. *Clin Exp Hypertens* 29: 13–21, 2007.
56. **Kimura Y, Hirooka Y, Kishi T, Ito K, Sagara Y, Sunagawa K.** Role of inducible nitric oxide synthase in rostral ventrolateral medulla in blood pressure regulation in spontaneously hypertensive rats. *Clin Exp Hypertens* 31: 281–286, 2009.
57. **Kishi T, Hirooka Y, Shigematsu H, Shimokawa H, Takeshita A.** Overexpression of eNOS in the RVLM causes hypotension and bradycardia via GABA release. *Hypertension* 38: 896–901, 2001.
58. **Kishi T, Hirooka Y, Ito K, Sakai K, Shimokawa H, Takeshita A.** Cardiovascular effects of overexpression of endothelial nitric oxide synthase in the rostral ventrolateral medulla in stroke-prone spontaneously hypertensive rats. *Hypertension* 39: 264–268, 2002.
59. **Kishi T, Hirooka Y, Mukai Y, Shimokawa H, Takeshita A.** Atorvastatin causes depressor and sympatho-inhibitory effect with upregulation of nitric oxide synthases in stroke-prone hypertensive rats. *J Hypertens* 21: 379–386, 2003.
60. **Kishi T, Hirooka Y, Kimura Y, Sakai K, Ito K, Shimokawa H, Takeshita A.** Overexpression of eNOS in RVLM improves impaired baroreflex control of heart rate in SHRSP. *Hypertension* 41: 255–260, 2003.
61. **Kishi T, Hirooka Y, Kimura Y, Ito K, Shimokawa H, Takeshita A.** Increased reactive oxygen species in rostral ventrolateral medulla contribute to neural mechanisms of hypertension in stroke-prone spontaneously hypertensive rats. *Circulation* 109: 2357–2362, 2004.
62. **Kishi T, Hirooka Y, Shimokawa H, Takeshita A, Sunagawa K.** Atorvastatin reduces oxidative stress in the rostral ventrolateral medulla of stroke-prone spontaneously hypertensive rats. *Clin Exp Hypertens* 30: 3–11, 2008.
63. **Kishi T, Hirooka Y, Konno S, Sunagawa K.** Atorvastatin improves the impaired baroreflex sensitivity via anti-oxidant effect in the rostral ventrolateral medulla of SHRSP. *Clin Exp Hypertens* 31: 698–704, 2009.
64. **Kishi T, Hirooka Y, Konno S, Sunagawa K.** Sympathoinhibition induced by centrally administered atorvastatin is associated with alteration of NAD(P)H and Mn-SOD activity in rostral ventrolateral medulla of stroke-prone SHR. *J Cardiovasc Pharmacol* 55: 184–190, 2010.
65. **Kishi T, Hirooka Y, Konno S, Ogawa K, Sunagawa K.** Angiotensin type 1 receptor-activated caspase-3 through ras/mitogen-activated protein kinase/extracellular signal-regulated kinase in the rostral ventrolateral medulla is involved in sympathoexcitation in stroke-prone spontaneously hypertensive rats. *Hypertension* 55: 291–297, 2010.
66. **Koga Y, Hirooka Y, Araki S, Nozoe M, Kishi T, Sunagawa K.** High salt intake enhances blood pressure increase during development of hypertension via oxidative stress in rostral ventrolateral medulla of spontaneously hypertensive rats. *Hypertens Res* 31: 2075–2083, 2008.
67. **Konno S, Hirooka Y, Araki S, Koga Y, Kishi T, Sunagawa K.** Azelnidipine decreases sympathetic nerve activity via antioxidant effect in the rostral ventrolateral medulla of stoke-prone spontaneously hypertensive rats. *J Cardiovasc Pharmacol* 52: 555–560, 2008.
68. **Kung LC, Chan SHH, Wu KLH, Ou CC, Tai MH, Chan JYH.** Mitochondrial respiratory enzyme complexes in rostral ventrolateral medulla as cellular targets of nitric oxide and superoxide interaction in the antagonism of antihypertensive action of eNOS transgene. *Mol Pharmacol* 74: 1319–1332, 2008.
69. **Kurukoff TL, Gehlen F, Ganten D, Wagner J.** Gene expression of brain nitric oxide synthase and soluble guanylate cyclase in hypothalamus and medulla of two-kidney, one-clip hypertensive rats. *Hypertension* 26: 171–176, 1995.
70. **Krukoff TL.** Central action of nitric oxide in regulation of autonomic functions. *Brain Res Rev* 30: 52–65, 1999.
71. **Lambeth JD.** Nox enzymes, ROS, and chronic disease: an example of antagonistic pleiotropy. *Free Radic Biol Med* 43: 332–347, 2007.
72. **Lassegue B, Clempus RE.** Vascular NAD(P)H oxidases: specific features, expression, and regulation. *Am J Physiol Regul Integr Comp Physiol* 285: R277–R297, 2003.
73. **Leenen FHH, Ruzicka M, Huang BS.** Central sympathoinhibitory effects of calcium channel blockers. *Curr Hypertens Res* 3: 314–321, 2001.
74. **Lin HC, Kang BH, Wan FJ, Huang ST, Tseng CJ.** Reciprocal regulation of nitric oxide and glutamate in the nucleus tractus solitarii of rats. *Eur J Pharmacol* 407: 83–89, 2000.
75. **Lin LH.** Glutamatergic neurons say NO in the nucleus tractus solitarii. *J Chem Neuroanat* 38: 1154–165, 2009.
76. **Lin Y, Matsumura K, Kagiyama S, Fukuhara M, Fujii K, Iida M.** Chronic administration of olmesartan attenuates the exaggerated pressor response to glutamate in the rostral ventrolateral medulla of SHR. *Brain Res* 1058: 161–166, 2005.
77. **Liu D, Gao L, Roy SK, Cornish KG, Zucker IH.** Neuronal angiotensin II type 1 receptor upregulation in heart failure: activation of activator protein 1 and jun N-terminal kinase. *Circ Res* 99: 1004–1011, 2006.
78. **Liu JL, Murakami H, Zucker IH.** Effects of NO on baroreflex control of heart rate and renal nerve activity in conscious rabbits. *Am J Physiol Regul Integr Comp Physiol* 270: R1361–R1370, 1996.
79. **Luft FC, Demmert G, Rohmeiss P, Unger T.** Baroreceptor reflex effect on sympathetic nerve activity in stroke-prone spontaneously hypertensive rats. *J Auton Nerv Syst* 17: 199–209, 1986.
80. **Ma S, Abboud FM, Felder RB.** Effects of L-arginine-derived nitric oxide synthesis on neuronal activity in nucleus tractus solitarius. *Am J Physiol Regul Integr Comp Physiol* 268: R487–R491, 1995.
81. **Marting-Pinge MC, Baraldi-Passy I, Lopes OU.** Excitatory effects of nitric oxide within the rostral ventrolateral medulla of freely moving rats. *Hypertension* 30: 704–707, 1997.
82. **Matsuo I, Hirooka Y, Hironaga K, Eshima K, Shigematsu H, Shihara M, Sakai K, Takeshita A.** Glutamate release via NO production evoked by NMDA in the NTS enhances hypotension and bradycardia in vivo. *Am J Physiol Regul Integr Comp Physiol* 280: R1285–R1291, 2001.
83. **McKinley MJ, Albinson AL, Allen AM, Mathai M, May CN, McAllen RM, Oldfield BJ, Mendelsohn FAO, Chai SY.** The brain renin-angiotensin system: location and physiological roles. *Int J Biochem Cell Biol* 35: 901–918, 2003.
84. **Mogi M, Horiuchi M.** Remote control of brain angiotensin II levels by angiotensin receptor blockers. *Hypertens Res* 33: 116–117, 2010.
85. **Morimoto S, Cassel MD, Beltz TG, Johnson AK, Davisson RL, Sigmund CD.** Elevated blood pressure in transgenic mice with brain-specific expression of human angiotensinogen driven by the glial fibrillary acidic protein promoter. *Circ Res* 89: 365–372, 2001.
86. **Morimoto S, Cassell MD, Sigmund CD.** The brain renin-angiotensin system in transgenic mice carrying a highly regulated human renin transgene. *Circ Res* 90: 80–86, 2002.
87. **Murakami H, Liu JL, Yoneyama H, Nishida Y, Okada K, Kosaka H, Morita H, Zucker IH.** Blockade of neuronal nitric oxide synthase alters the baroreflex control of heart rate in the rabbit. *Am J Physiol Regul Integr Comp Physiol* 274: R181–R186, 1998.
88. **Murphy S, Gibson CL.** Nitric oxide, ischaemia and brain inflammation. *Biochem Soc Trans* 35: 1133–1137, 2007.
89. **Nishimura Y, Ito T, Hoe KL, Saavedra JM.** Chronic peripheral administration of the angiotensin II AT_1 receptor antagonist candesartan blocks brain AT_1 receptors. *Brain Res* 871: 29–38, 2000.
90. **Nozoe M, Hirooka Y, Koga Y, Sagara Y, Kishi T, Engelhardt JF, Sunagawa K.** Inhibition of rac1-derived reactive oxygen species in nucleus tractus solitarius decreases blood pressure and heart rate in stroke-prone spontaneously hypertensive rats. *Hypertension* 50: 62–68, 2007.
91. **Nozoe M, Hirooka Y, Koga Y, Araki S, Konno S, Kishi T, Ide T, Sunagawa K.** Mitochondria-derived reactive oxygen species mediate sympathoexcitation induced by angiotensin II in the rostral ventrolateral medulla. *J Hypertens* 26: 2176–2184, 2008.
92. **Oliveira-Sales EB, Dugaich AP, Carillo BA, Abreu NP, Boim MA, Martins PJ, D'Almeida V, Dolnkoff MS, Bergamaschi CT, Campos RR.** Oxidative stress contributes to renovascular hypertension. *Am J Hypertens* 21: 98–104, 2008.
93. **Oliveira-Sales EB, Nishi EE, Carillo BA, Dolnikoff MS, Bergamaschi CT, Campos RR.** Oxidative stress in the sympathetic premotor neurons contributes to sympathetic activation in renovascular hypertension. *Am J Hypertens* 22: 484–492, 2009.
94. **Paravicini T, Touyz RM.** Redox signaling in hypertension. *Cardiovasc Res* 71: 247–258, 2006.
95. **Patel KP, Li YF, Hirooka Y.** Role of nitric oxide in central sympathetic outflow. *Exp Biol Med (Maywood)* 226: 814–824, 2001.

96. **Paton JFR, Waki H, Abdala APL, Dickinson J, Kasparov S.** Vascular-brain signaling in hypertension: role of angiotensin II and nitric oxide. *Curr Hypertens Rep* 9: 242–247, 2007.
97. **Pannu R, Singh I.** Pharmacological strategies for the regulation of inducible nitric oxide synthase: neurogenerative versus neuroprotective mechanisms. *Neurochem Intl* 49: 170–182, 2006.
98. **Pelisch N, Hosomi N, Ueno M, Masugata H, Murao K, Hitomi H, Nakao D, Kobori H, Nishiyama A, Kohno M.** Systemic candesartan reduces brain angiotensin II via downregulation of brain renin-angiotensin system. *Hypertens Res* 33: 161–164, 2010.
99. **Peterson JR, Shrama RV, Davisson RL.** Reactive oxygen species in the neuropathogenesis of hypertension. *Curr Hypertens Rep* 8: 232–241, 2006.
100. **Pilowsky P, Goodchild AK.** Baroreceptor reflex pathways and neurotransmitters: 10 years on. *J Hypertens* 20: 1675–1688, 2002.
101. **Plochocka-Zulinska D, Krukoff TL.** Increased gene expression of neuronal nitric oxide synthase in brain of adult spontaneously hypertensive rats. *Mol Brain Res* 48: 291–297, 1997.
102. **Polizio AH, Peña C.** Effects of angiotensin II type 1 receptor blockade on the oxidative stress in spontaneously hypertensive rat tissues. *Regul Pept* 128: 1–5, 2005.
103. **Pontieri V, Venezuela MK, Scavone C, Michelini LC.** Role of endogenous nitric oxide in the nucleus tractus solitarii on baroreflex control of heart rate in spontaneously hypertensive rats. *J Hypertens* 16: 1993–1999, 1998.
104. **Qadri F, Arens T, Schwarz EC, Häuser W, Dendorfer A, Dominiak P.** Brain nitric oxide synthase activity in spontaneously hypertensive rats during development of hypertension. *J Hypertens* 21: 1687–1694, 2003.
105. **Reja V, Goodchild AK, Phillips JK, Pilowski PM.** Upregulation of angiotensin AT_1 receptor and intracellular kinase gene expression in hypertensive rats. *Clin Exp Pharmacol Physiol* 33: 690–695, 2006.
106. **Ren J.** Influence of gender on oxidative stress, lipid peroxidation, protein damage and apoptosis in hearts and brains from spontaneously hypertensive rats. *Clin Exp Pharmacol Physiol* 34: 432–438, 2007.
107. **Sakai K, Hirooka Y, Matsuo I, Eshima K, Shigematsu H, Shimokawa H, Takeshita A.** Overexpression of eNOS in NTS causes hypotension and bradycardia in vivo. *Hypertension* 36: 1023–1028, 2000.
108. **Sakai K, Agassandian K, Morimoto S, Sinnayah P, Cassell MD, Davisson RL, Sigmund CD.** Local production of angiotensin II in the subfornical organ causes elevated drinking. *J Clin Invest* 117: 1088–1095, 2007.
109. **Sander M, Chavoshan B, Victor RG.** A large blood pressure-raising effect of nitric oxide synthase inhibition in humans. *Hypertension* 33: 937–942, 1999.
110. **Sano H, Matsumoto K, Utsumi H.** Synthesis and imaging of blood-brain-barrier permeable nitroxyl-probes for free radicals reactions in brain of living mice. *Biochem Mol Biol Int* 42: 641–647, 1997.
111. **Sano H, Naruse M, Matsumoto K, Oi T, Utsumi H.** A new nitroxy-probe with high retention in the brain and its application for brain imaging. *Free Radic Biol Med* 28: 959–969, 2000.
112. **Shapoval LN, Sagach VF, Pobegailo LS.** Nitric oxide influences ventrolateral medullary mechanisms of vasomotor control in the cat. *Neurosci Lett* 132: 47–50, 1991.
113. **Sun C, Sellers KW, Sumners C, Raizada MK.** NAD(P)H oxidase inhibition attenuates neuronal chronotropic actions of angiotensin II. *Circ Res* 96: 659–666, 2005.
114. **Sun J, Druhan LJ, Zweier JL.** Reactive oxygen and nitrogen species regulate inducible nitric oxide synthase function shifting the balance of nitric oxide and superoxide production. *Arch Biochem Biophys* 494: 130–137, 2010.
115. **Sved AF, Ito S, Sved JC.** Brainstem mechanisms of hypertension: role of the rostral ventrolateral medulla. *Curr Hypertens Rep* 5: 262–268, 2003.
116. **Tagawa T, Imaizumi T, Harada S, Endo T, Shiramoto M, Hirooka Y, Takeshita A.** Nitric oxide influences neuronal activity in the nucleus tractus solitarius of rat brainstem slices. *Circ Res* 75: 70–76, 1994.
117. **Tai MH, Wang LL, Wu KLH, Chan JYH.** Increased superoxide anion in rostral ventrolateral medulla contributes to hypertension in spontaneously hypertensive rats via interactions with nitric oxide. *Free Radic Biol Med* 38: 450–462, 2005.
118. **Talman WT, Dragon DN.** Transmission of arterial baroreflex signals depends on neuronal nitric oxide synthase. *Hypertension* 43: 820–824, 2004.
119. **Talman WT.** NO and central cardiovascular control: a simple molecule with a complex story. *Hypertension* 48: 552–554, 2006.
120. **Tseng CJ, Liu HY, Lin HC, Ger LP, Tung CS, Yen MH.** Cardiovascular effects of nitric oxide in the brain stem nuclei of rats. *Hypertension* 27: 36–42, 1996.
121. **Waki H, Murphy D, Yao ST, Kasparov S, Paton JFR.** Endothelial NO synthase activity in nucleus tractus solitarii contributes to hypertension in spontaneously hypertensive rats. *Hypertension* 48: 644–650, 2006.
122. **Wang G, Anrather J, Huang J, Speth RC, Pickel VM, Iadecola C.** NADPH oxidase contributes angiotensin signaling in the nucleus tractus solitarius. *J Neurosci* 24: 5516–5524, 2004.
123. **Wang G, Anrather J, Glass MJ, Tarsitano J, Zhou P, Frys KA, Pickel VM, Iadecola C.** Nox2, Ca^{2+}, and protein kinase C play a role in angiotensin II-induced free radical production in nucleus tractus solitarius. *Hypertension* 48: 482–489, 2006.
124. **Wang JM, Tan J, Leenen FHH.** Central nervous system blockade by peripheral administration of AT_1 receptor blockers. *J Cardiovasc Pharmacol* 41: 593–599, 2003.
125. **Wang S, Paton JFR, Kasparov.** Differential sensitivity of excitatory and inhibitory synaptic transmission to modulation by nitric oxide in rat nucleus tractus solitarii. *Exp Physiol* 92: 371–382, 2007.
126. **Wu SY, Dun NJ.** Potentiation of IPSCs by nitric oxide in immature rat sympathetic preganglionic neurons in vitro. *J Physiol* 495: 479–490, 1996.
127. **Wu SY, Dun NJ.** Nitric oxide and excitatory postsynaptic currents in immature rat sympathetic preganglionic neurons in vitro. *Neuroscience* 79: 237–245, 1997.
128. **Yin JX, Yang RF, Li S, Renshaw AO, Li YL, Schultz HD, Zimmerman MC.** Mitochondria-produced superoxide mediates angiotensin II-induced inhibition of neuronal potassium current. *Am J Physiol Cell Physiol* 298: C857–C865, 2010.
129. **Zanzinger J.** Role of nitric oxide in the neural control of cardiovascular function. *Cardiovasc Res* 43: 639–649, 1999.
130. **Zanzinger J.** Mechanisms of action of nitric oxide in the brain stem: role of oxidative stress. *Auton Neurosci* 98: 24–27, 2002.
131. **Zanzinger J, Czachurski J, Seller H.** Inhibition of basal and reflex-mediated sympathetic activity in the RVLM by nitric oxide. *Am J Physiol Regul Integr Comp Physiol* 268: R958–R962, 1995.
132. **Zimmerman MC, Lazartigues E, Lang JA, Sinnayah P, Ahmad IM, Spitz DR, Davisson RL.** Superoxide mediates the actions of angiotensin II in the central nervous system. *Circ Res* 91: 1038–1045, 2002.
133. **Zimmerman MC, Lazartigues E, Sharma RV, Davisson RL.** Hypertension caused by angiotensin II infusion involves increased superoxide production in the central nervous system. *Circ Res* 95: 210–216, 2004.
134. **Zimmerman MC, Dunlay RP, Larzartigues E, Zhang Y, Sharma RV, Engelhardt JF, Davisson RL.** Requirement for Rac-1dependent NADPH oxidase in the cardiovascular and dipsogenic actions of angiotensin II in the brain. *Circ Res* 95: 532–539, 2004.
135. **Zimmerman MC, Sharma RV, Davisson RL.** Superoxide mediates angiotensin II-induced influx of extracellular calcium in neural cells. *Hypertension* 45: 717–723, 2005.
136. **Zimmerman MC, Zucker IH.** Mitochondrial dysfunction and mitochondrial-produced reactive oxygen species: new targets for neurogenic hypertension? *Hypertension* 53: 112–114, 2009.

Nanoparticle-Mediated Delivery of Pitavastatin Into Lungs Ameliorates the Development and Induces Regression of Monocrotaline-Induced Pulmonary Artery Hypertension

Ling Chen, Kaku Nakano, Satoshi Kimura, Tetsuya Matoba, Eiko Iwata, Miho Miyagawa, Hiroyuki Tsujimoto, Kazuhiro Nagaoka, Junji Kishimoto, Kenji Sunagawa, Kensuke Egashira

Abstract—Pulmonary artery hypertension (PAH) is an intractable disease of the small PAs in which multiple pathogenic factors are involved. Statins are known to mitigate endothelial injury and inhibit vascular remodeling and inflammation, all of which play crucial roles in the pathogenesis of PAH. We tested the hypothesis that nanoparticle (NP)-mediated delivery of pitavastatin into the lungs can be a novel therapeutic approach for the treatment of PAH. Among the marketed statins, pitavastatin was found to have the most potent effects on proliferation of PA smooth muscle cells in vitro. We formulated pitavastatin-NP and found that pitavastatin-NP was more effective than pitavastatin alone in inhibiting cellular proliferation and inflammation in vitro. In a rat model of monocrotaline-induced PAH, a single intratracheal instillation of NP resulted in the delivery of NP into alveolar macrophages and small PAs for up to 14 days after instillation. Intratracheal treatment with pitavastatin-NP, but not with pitavastatin, attenuated the development of PAH and was associated with a reduction of inflammation and PA remodeling. NP-mediated pitavastatin delivery was more effective than systemic administration of pitavastatin in attenuating the development of PAH. Importantly, treatment with pitavastatin-NP 3 weeks after monocrotaline injection induced regression of PAH and improved survival rate. This mode of NP-mediated pitavastatin delivery into the lungs is effective in attenuating the development of PAH and inducing regression of established PAH, suggesting potential clinical significance for developing a new treatment for PAH. (***Hypertension*. 2011;57:343-350.**) • **Online Data Supplement**

Key Words: pulmonary hypertension ■ nanotechnology ■ pitavastatin ■ inflammation ■ leukocytes

Pulmonary artery hypertension (PAH) is an intractable disease of the small PAs resulting in progressive increases in pulmonary vascular resistance, right ventricular (RV) failure, and ultimately premature death.[1,2] Mortality from PAH remains high, even after introduction of vasodilator therapies such as prostacyclin infusion, endothelin receptor antagonists, and phosphodiesterase inhibitors (which have raised the 5-year survival rate to ≈50%). Although these drugs were originally developed for non-PAH vascular diseases, they were introduced into treatment for clinical PAH on the basis of the vasodilator hypothesis. Therefore, a new idea that might lead to a breakthrough curative treatment for PAH is urgently needed.

In addition to vasoconstriction, other multiple factors (endothelial injury/apoptosis, obstructive vascular remodeling, proliferation, and inflammation) play an important role in the mechanism of PAH.[1,2] Therefore, we hypothesized that a controlled, local delivery system targeting a battery of those pathogenic factors intrinsic to PAH pathology would be a favorable therapeutic approach with high translational potential to clinical medicine. In this respect, we focused on the vasculoprotective effects of 3-hydroxy-3-methylglutaryl coenzyme A reductase inhibitors, the so-called statins. Statins are known to increase expression and activity of endothelial nitric oxide synthase (eNOS) and thus ameliorate endothelial injury.[3–6] Prior studies have reported that systemic administration of statins attenuates monocrotaline (MCT)-induced and hypoxia-induced PAH in animals.[7–9] These beneficial therapeutic effects of statins on PAH, however, were observed after daily administration of high doses of statins, a regimen that could lead to serious adverse side effects in the clinical setting. However, not all studies have reported beneficial effects of statins with regard to PAH in animal models.[10,11] We recently reported that (1) intratracheal administration of bioabsorbable polymeric nanoparticles (NPs) represented a novel drug delivery system into the lung; and (2) NP-mediated delivery of a nuclear factor (NF)-κB decoy into the lungs effectively inhibited NF-κB–mediated inflammation and thus, attenuated the development and progression of PAH in a rat model of MCT-induced PAH.[12] This

Received May 23, 2010; first decision June 21, 2010; revision accepted December 8, 2010.

From the Department of Cardiovascular Medicine (L.C., K.N., T.M., E.I., M.M., K.N., K.S., K.E.) and Digital Medicine Initiative (J.K.), Graduate School of Medical Science, Kyushu University, Fukuoka, and Hosokawa Micron Corporation (H.T.), Osaka, Japan.

Correspondence to Kensuke Egashira, Department of Cardiovascular Medicine, Graduate School of Medical Science, Kyushu University, 3-1-1, Maidashi, Higashi-ku, Fukuoka 812-8582, Japan. E-mail egashira@cardiol.med.kyushu-u.ac.jp

Hypertension **is available at http://hyper.ahajournals.org** **DOI: 10.1161/HYPERTENSIONAHA.110.157032**

nanotechnology platform may optimize the efficacy and minimize the potential side effects of drugs.

Therefore, the primary aim of this study was to test the hypothesis that NP-mediated local delivery of statins to the lung is an innovative therapeutic approach for PAH. Pitavastatin was selected as the nanoparticulation compound because this drug has shown the most potent beneficial effects on human endothelial and smooth muscle cells in vitro compared with other statins.[13,14] We then used a rat model of MCT-induced PAH and examined (1) whether this NP-mediated delivery of pitavastatin into the lung is more effective than intratracheal or systemic administration of pitavastatin in attenuating the development of PAH and (2) whether this NP-mediated delivery system induces regression of established PAH.

Materials and Methods

Human PA Smooth Muscle Cell Proliferation Assay

Human PA smooth muscle cells (PASMCs) were seeded on 96-well culture plates at 10^4 cells per well in SmBM. After 24 hours of starvation, 10% fetal bovine serum was added for cell stimulation. In addition, various concentrations of statins (simvastatin, pitavastatin, atorvastatin, losuvastatin, fluvastatin, and pravastatin) or vehicle were added (n=6 per group). Statins were purchased, extracted from products, and purified. Cells were incubated for another 24 hours after addition of 5′-bromo-2′-deoxyuridine, and 5′-bromo-2′-deoxyuridine incorporation was evaluated by an ELISA kit from Calbiochem.

In another set of experiments, a 1.0-mL suspension of pitavastatin at 5 mg/mL, fluorescein isothiocyanate (FITC)–NP (1 mg/mL lactide/glycolide copolymer [PLGA]), pitavastatin-NP containing 1.0 mg/mL PLGA and 5 mg/mL pitavastatin, or vehicle was added to each well (n=6 per group). Cells were incubated for another 4 days, and the cells were fixed with methanol and stained with Diff-Quick staining solution. A single observer counted the number of cells per plate.

Preparation of PLGA-NP

A PLGA with an average molecular weight of 20 000 and a copolymer ratio of lactide to glycolide of 75:25 (Wako Pure Chemical Industries, Osaka, Japan) was used as wall material for the NP. PLGA-NP incorporated with FITC or pitavastatin (Kowa Pharmaceutical Co Ltd, Tokyo, Japan) was prepared by a previously reported emulsion solvent diffusion method in purified water.[15,16] PLGA was dissolved in a mixture of acetone and methanol. Then, FITC or pitavastatin was added to this solution. The resultant PLGA-FITC or PLGA-statin solution was emulsified in a polyvinyl alcohol solution with stirring at 400 rpm by using a propeller-type agitator with 3 blades (Heidon 600G, Shinto Scientific, Tokyo, Japan). After the system was agitated for 2 hours under reduced pressure at 40°C, the entire suspension was centrifuged (20 000*g* for 20 minutes at −20°C). After the supernatant was removed, purified water was added and mixed with the sediment. The wet mixture was then centrifuged again to remove the excess polyvinyl alcohol and the unencapsulated reagent that could not adsorb onto the surfaces of the NPs. After this process was repeated, the resultant dispersion was freeze-dried under the same conditions. The FITC- and pitavastatin-loaded PLGA-NP contained 13% (wt/vol) FITC and 13% (wt/vol) pitavastatin, respectively. A sample of NP suspension in distilled water was used for particle size analysis. The diameter of NPs was 196±29 nm. Surface charge (zeta potential) was also analyzed by Zetasizer Nano (Sysmex, Hyogo, Japan) and was anionic (−15±10 mV at pH 4.4).

Experimental Animal Models

All experiments were reviewed and approved by the committee on ethics on animal experiments, Kyushu University Faculty of Medicine, and were conducted according to the guidelines of the American Physiological Society. Adult male Sprague-Dawley rats (Charles River, Yokohama, Japan; 250 to 300 g body weight) were injected subcutaneously with 60 mg/kg MCT (Wako), which induces severe PAH in 3 weeks.[12,17]

In a prevention protocol, animals were divided into 4 groups that received intratracheal instillation of phosphate-buffered saline (PBS), pitavastatin only (100 μg), FITC-NP (1 mg PLGA), or pitavastatin-NP (100 μg pitavastatin per mg PLGA) immediately after MCT injection. For intratracheal instillation, a 0.1-mL suspension of pitavastatin, FITC-NP, or pitavastatin-NP was injected gently into the trachea of animals, accompanied by an equal volume of air. This dose of pitavastatin was selected because we examined the effects of intratracheal instillation of various concentrations and volumes of pitavastatin suspension (10, 30, 100, or 300 μg per animal in 0.05, 0.1, and 0.2 mL PBS) and confirmed that a 0.1-mL suspension of pitavastatin containing 100 μg pitavastatin was an optimal dose in our experiments. In a treatment protocol, rats were divided into 4 groups that received intratracheal instillation of PBS, pitavastatin only (100 μg), FITC-NP (1 mg PLGA), or pitavastatin-NP (100 μg pitavastatin per mg PLGA) 21 days after MCT injection when severe PAH had already been established. In another set of experiments, 3 other groups received systemic daily oral pitavastatin at doses of 0.3, 1.0, 3.0, and 10 mg/kg, dissolved in 0.5% carboxymethyl cellulose, by gavage from the day of MCT injection until the mice were euthanized on day 21.

Biodistribution of FITC-NP After Intratracheal Administration Into the Lung

Biodistribution of FITC in the lung was examined in rats that received intratracheal instillation of FITC-NP. Animals were euthanized and the tracheas were exposed. The lungs were inflated with a solution of 10% phosphate-buffered formalin (pH 7.4) by using a catheter inserted into the trachea. The lungs were then removed en bloc and placed into 10% phosphate-buffered formalin for a further 12 to 18 hours. After light and fluorescence stereoscopic photographs of the lungs were taken, the tissues were processed and embedded in OCT compound, and cross sections of 5-μm thickness were prepared for detecting NP distribution by fluorescence photomicroscopy. The tissue specimens were also processed and embedded in paraffin according to standard procedures, and 5-μm sections were cut. Sections were further examined to detect NP distribution by immunostaining.

Direct RV Pressure Measurements

Three weeks after MCT administration, the animals were anesthetized with sodium pentobarbital, and polyethylene catheters were then inserted into the right ventricle through the jugular vein and carotid artery for hemodynamic measurements. RV systolic pressure and systemic blood pressure were measured with a polygraph system (AP-601G, Nihon Kohden).[12,17]

Echocardiographic Measurements of RV and PA Hemodynamics

Transthoracic echocardiographic measurements (Vevo 2100 ultrasound system; Primetech Inc) were performed as described previously.[18] Additional details are provided in the online-only Data Supplement (available at http://hyper.ahajournals.org).

Assessment of Right Heart Hypertrophy and PA Remodeling

After systemic arterial and RV pressures were recorded, the animals were euthanized and the lungs and heart were isolated. The RV wall was dissected from the left ventricle and ventricular septum. Wet weight of the right ventricle and of the left ventricle plus ventricular

septum was determined, and RV hypertrophy was expressed as RV weight/(left ventricle plus ventricular septum weights).[12,17]

The lungs were perfused with a solution of 10% phosphate-buffered formalin (pH 7.4). At the same time, 10% phosphate-buffered formalin (pH 7.4) was administered into the lungs via tracheal tube at a pressure of 20 cm H_2O. These specimens were processed for light microscopy by routine paraffin embedding. The degree of remodeling (muscularization) of small, peripheral, PAs was assessed by double immunohistochemical staining of the 5-μm sections with an anti–α-smooth muscle actin antibody (dilution 1:500; clone 1A4, Dako) and anti-platelet endothelial cell adhesion molecule-1 (PECAM-1) (M-20) antibody (dilution 1:100, Santa Cruz).[12] To assess the type of remodeling of muscular PAs, microscopic images were analyzed. In each rat, 30 to 40 intra-acinar arteries were categorized as muscular (those with a complete medial coat of muscle), partially muscular (those with only a crescent of muscle), or nonmuscular (those with no apparent muscle), counted, and averaged within a range of diameters from 25 to 50 μm.[12]

Histopathologic and Immunohistochemical Analysis of Rat Lungs

The degrees of monocyte infiltration were evaluated by immunostaining for ED-1 (analog of human CD68, Serotec). For quantification, a blinded observer counted the number of ED-1–positive cells in 10 fields. Sections were also subjected to immunostaining with antibodies against FITC (1:1000; American Research Products, Belmont, MA), an epitope (α-p65) on the p65 subunit of NF-κB (1:100; Boehringer Mannheim, Roche Diagnostics, Basel, Switzerland), rabbit eNOS (ABR: PA1–037), murine inducible NOS (iNOS, Transduction Laboratories), or nonimmune mouse IgG (Dako). The α-p65 monoclonal antibody recognizes an epitope on the p65 subunit that is masked by bound inhibitor-κB.[19] Therefore, this antibody exclusively detects activated NF-κB.[19]

Real-Time Quantitative Reverse Transcription–Polymerase Chain Reaction

Real-time polymerase chain reaction amplification was performed with rat cDNA with the use of an ABI PRISM 7000 sequence detection system (Applied Biosystems, Foster City, CA) as described previously.[12,19] TaqMan primers/probes for monocyte chemotactic protein-1, tumor necrosis factor-α, interleukin (IL)-1β, IL-6, intercellular adhesion molecule-1, and glyceraldehyde 3-phosphate dehydrogenase, which served as the endogenous reference, were purchased from Applied Biosystems (Assay-on-Demand gene expression products Rn00580555, Rn99999017, Rn00580432, Rn00561420, and Rn00564227 and TaqMan rodent glyceraldehyde 3-phosphate dehydrogenase control reagents, respectively).

Lipopolysaccharide-Induced Activation of Mouse Monocytes

The mouse macrophage cell line RAW 264.7 was purchased. After bacterial lipopolysaccharide (serotype 0111:B4, Sigma) at 1 μg/mL was added to the cells, each 1.0-mL suspension of pitavastatin at 5 mg/mL, FITC-NP (1 mg/mL PLGA), pitavastatin-NP containing 1.0 mg/mL PLGA and 5 mg/mL pitavastatin, or vehicle was added to the wells; 2 hours later, the cells were washed 3 times with PBS. NF-κB pathway activity was measured with a TransAM NF-κB p65 ELISA-based assay kit (Active Motif, Tokyo, Japan). Nuclear extracts of RAW 264.7 cells were prepared with the NE-PER nuclear and cytoplasmic extraction reagent kit (Pierce, Rockford, IL) according to the manufacture's protocol. Samples were placed, along with 30 μL of binding buffer, on a 96-well plate to which oligonucleotides containing an NF-κB consensus binding site had been immobilized for 1 hour on a shaker. During this time, the activated NF-κB contained in the sample specifically binds to this nucleotide; then the plate was washed and, by using a primary antibody (100 mL diluted 1:1000 in antibody binding buffer for 1 hour) that is directed against the NF-κB p65 subunit, the NF-κB complex bound to the oligonucleotides can be detected. The plate was then washed again, and 100 μL of secondary antibody (diluted 1:1000 in antibody binding buffer) conjugated to horseradish peroxidase was added for 1 hour. The plate was washed again, and 100 μL of developing solution was added. The plate was incubated for 4 minutes away from direct light, 100 μL of stop solution was added, and the plate was read with a plate reader at 450 nm.

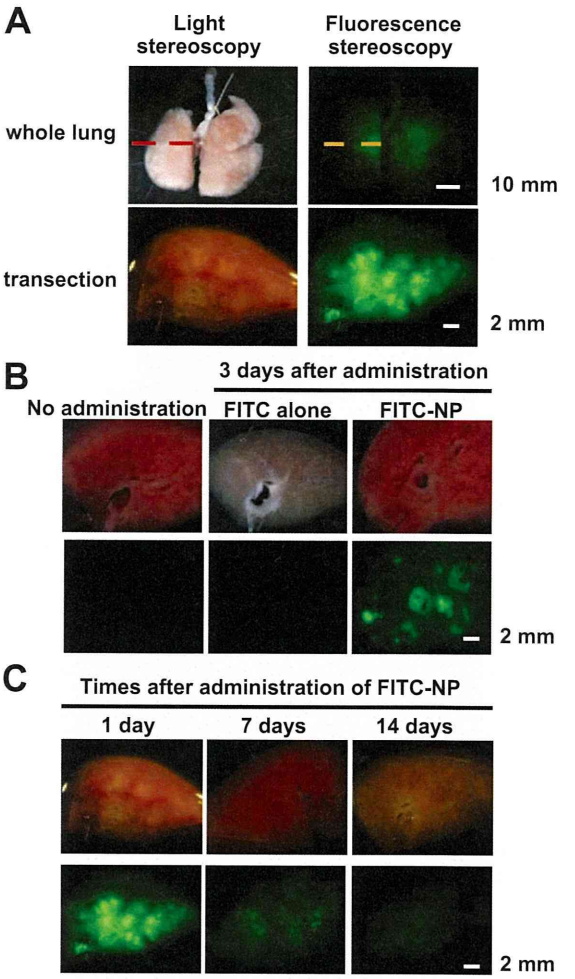

Figure 1. Localization of FITC-NP after instillation into the rat lung. A, Representative light (left) and fluorescence (right) stereomicrographs of whole lungs (upper) and transections (lower) 1 hour after intratracheal instillation of FITC-NP. B, Representative light (upper) and fluorescence (lower) stereomicrographs of transections from control (nontreated) lungs and from lungs instillated with FITC alone or FITC NP on day 3 after instillation. C, Representative light (upper) and fluorescence (lower) stereomicrographs of cross sections from lungs instillated with FITC-NP on days 1, 7, and 14 after instillation.

Western Blot Analysis

Protein was extracted from frozen lung tissues. Samples were homogenized in lysis buffer containing 10 mmol/L Tris-HCl, pH 7.4, 50 mmol/L NaCl, 5 mmol/L EDTA, 1% Triton X-100, 50 mmol/L NaCl, 30 mmol/L sodium phosphate, 50 mmol/L NaF, 1% aprotinin, 0.5% pepstatin A, 2 mmol/L phenylmethylsulfonyl fluoride, and 5 mmol/L leupeptin and phosphatase inhibitor cocktail (Pierce). Cell lysates (50 μg) were separated on 7.5% polyacrylamide gels and blotted onto polyvinylidene difluoride membranes (Millipore Co, Hercules, CA). Protein expression was analyzed by using antibodies against eNOS (ABR: PA1–037) or actin (Sigma). Immune complexes were visualized with horseradish peroxidase–conjugated secondary antibodies. Bound antibodies were detected by chemiluminescence with the use of an ECL detection system (Amersham Biosciences) and quantified by densitometry.

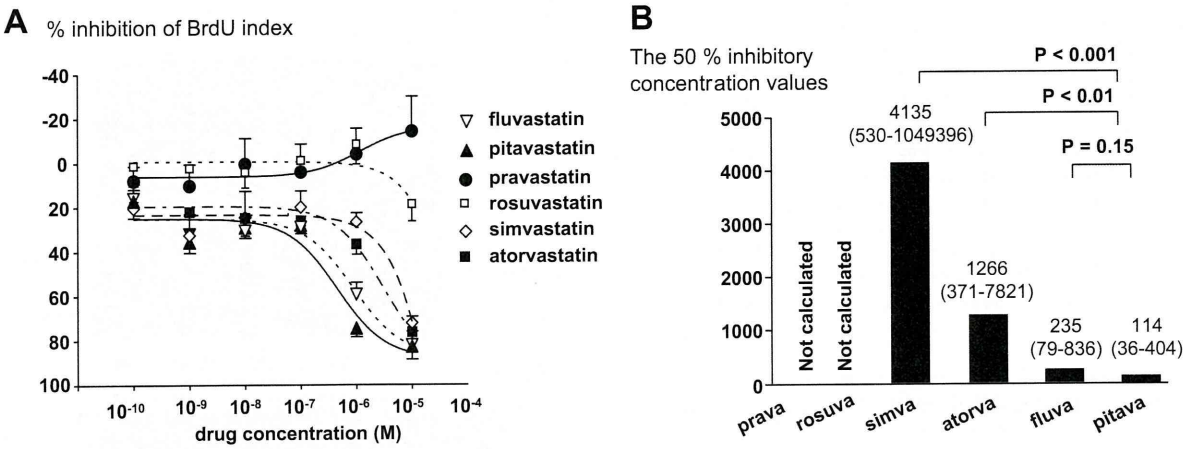

Figure 2. Inhibitory effects of various statins on human PASMC proliferation. A, PASMC proliferation assay (% inhibition of 5′-bromo-2′-deoxyuridine [BrdU] index) in response to various concentrations of various statins (n=6 per group). B, IC_{50} values and 95% Wald CIs (in parentheses) are shown at the top of each bar. Probability values vs pitavastatin by Wald tests in a 4-parameter logistic-regression model are shown. Prava indicates pravastatin; rosuva, rosuvastatin; simva, simvastatin; atorva, atorvastatin; fluva, fluvastatin; and pitava, pitavastatin.

Measurements of Pitavastatin Concentration

Pitavastatin concentrations in serum and lung were measured at predetermined time points by using a column-switching high-performance liquid chromatography system, as previously reported.[20] In brief, the column-switching high-performance liquid chromatography system consists of 2 LC-10AD pumps, an SIL-10A autosampler, a CTO-10A column oven, a 6-port column-switching valve, and an SPD-10A UV detector (all from Shimadzu, Kyoto, Japan). The column temperature was maintained at 40°C. Preprepared serum or tissue homogenate sample solutions were injected from the autosampler into the high-performance liquid chromatography system, and detection of the statin in sample solutions was performed at 250 nm with a UV detector. The detected peak area was measured with Lcsolution software (Shimadzu).

Statistical Analysis

Data are presented as mean±SEM. Statistical analysis of differences was performed by 1-way ANOVA and Bonferroni's multiple comparison tests. The survival rates were determined by the Kaplan-Meier method. Efficacy ratios (median inhibitory concentration [IC_{50}]values) of statins were tested with Wald tests in a 4-parameter logistic-regression model. Point estimates and Wald 95% CIs for IC_{50} values were calculated. Statistical calculations were performed with SAS preclinical package software version 9.1.3 (SAS Institute Inc, Tokyo, Japan) and Prism Software version 4.0.1 (GrafPad). A value of $P<0.05$ was considered statistically significant.

Results

Localization of FITC-NP in the Lung of Rats With MCT-Induced PAH

Localization of FITC was examined after a single intratracheal instillation of FITC-NP into animals injected with MCT. Three days after instillation, strong FITC signals were detected only in FITC-NP–instillated lungs, whereas no or only faint FITC signals were observed in control noninjected lungs and in lungs injected with FITC only (Figure 1). On days 1, 7, and 14, FITC signals remained localized predominantly in the lungs. There were FITC-positive cells in the bronchi and alveoli, alveolar macrophages, and small arteries. As we previously reported,[12] immunofluorescence staining revealed that FITC signals localized mainly in small arteries and arterioles as well as in small bronchi and alveoli 14 days after instillation of FITC-NP (online-only Figure I). FITC signals were not detected in remote organs (liver, spleen, and heart) at any time point (data not shown).

Inhibitory Effects of Statins on Human PASMC Proliferation

To implicate pitavastatin as a candidate statin for nanoparticulation, the effects of statins on PASMC proliferation were examined. In a human PASMC proliferation assay (percent inhibition of 5′-bromo-2′-deoxyuridine index), hydrophilic statins (rosuvastatin and pravastatin) elicited no inhibitory effects, whereas other statins showed dose-dependent effects (Figure 2A). The IC_{50} value of pitavastatin was lower than that of simvastatin or atorvastatin (Figure 2B). The IC_{50} value of pitavastatin tended to be lower than that of fluvastatin, but there was no significant difference in the IC_{50} values between the 2 statins.

Effects of Pitavastatin-NP on the Development of PAH in the Rat Model of MCT-Induced PAH

An RV catheterization study confirmed that injection of MCT led to severe PAH (increased RV systolic pressure) associated with small PA remodeling and increased infiltration of ED1-positive monocytes 3 weeks after MCT injection, as previously reported.[12,17] Single intratracheal treatment with pitavastatin-NP, but not with pitavastatin alone or FITC-NP, attenuated the development of PAH, small PA remodeling, and monocyte-mediated inflammation (Figure 3). The RV systolic pressure of untreated normal controls (no MCT injection) was 34±2 mm Hg (n=10). There were no significant differences in concentrations of pitavastatin in the lung and systemic blood between pitavastatin-NP–treated and pitavastatin-only groups (the Table).

Echocardiographic study showed that there were no significant changes in cardiac output or stroke volume among untreated control and MCT-induced PAH rats (online-only Table I). Echo-derived estimation of RV systolic pressure and pulmonary vascular resistance showed the development of MCT-induced PAH and therapeutic effects of a single intra-

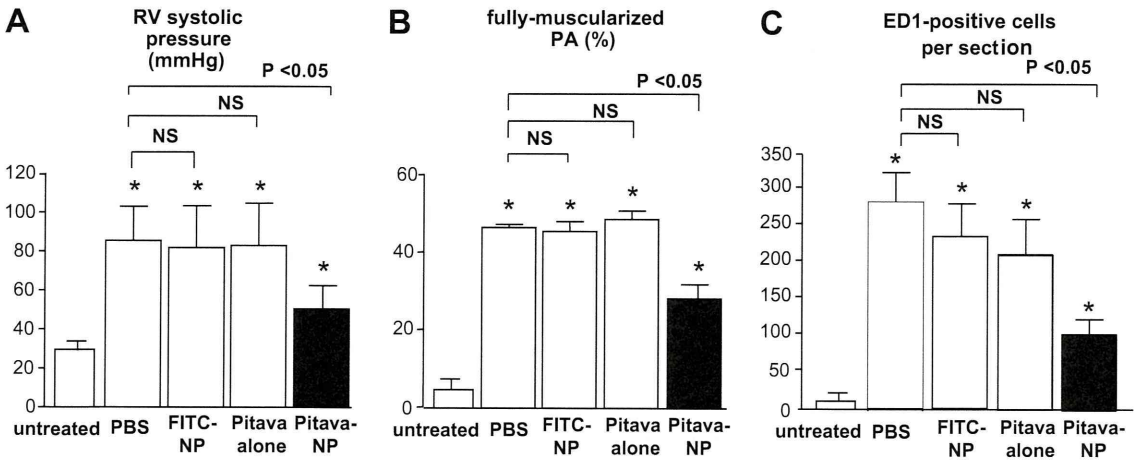

Figure 3. Effects of pitavastatin (pitava)-NP on RV systolic pressure, small PA remodeling, and infiltration of monocytes 3 weeks after MCT injection. A, RV systolic pressure in the 4 experimental groups. Data are mean±SEM (n=6 per group). B, Percentage of fully muscularized small PAs in the 4 experimental groups. Data are mean±SEM (n=6 per group). C, Infiltration of ED1-positive monocytes into the lung (the number of positive cells per 30 high-power-field cross sections). Data are mean±SEM (n=6 per group). *$P<0.01$ vs untreated control.

tracheal instillation of pitavastatin-NP, as reported by the RV catheterization study.

The activity of lactate dehydrogenase was not detected in bronchoalveolar lavage fluid. There were no significant changes in activity of lactate dehydrogenase and various biomarkers in lung tissue homogenates among untreated control and MCT-induced PAH rats (online-only Tables II and III).

Oral daily administration of pitavastatin at 0.3 mg/kg had no significant effects on MCT-induced PAH, but pitavastatin at 1.0, 3.0, and 10 mg/kg significantly attenuated the development of PAH (online-only Figure II).

Effects of Intratracheal Instillation of Pitavastatin-NP on NF-κB Activation and PAMSC Proliferation

As previously reported,[12] immunohistochemically detectable NF-κB activation was noted mainly in alveolar macrophages and weakly in PA lesions 7 days after MCT administration (Figure 4). A single intratracheal instillation of pitavastatin-NP, but not of FITC-NP or pitavastatin alone, markedly attenuated the increases in NF-κB (α-p65) activity induced by MCT injection (Figure 4). Because NF-κB was activated in alveolar monocytes in MCT-induced PAH, effects of pitavastatin-NP on NF-κB activity were examined in a monocyte cell line (RAW 264.7 cells) in vitro. Treatment with pitavastatin-NP, but not with pitavastatin only, attenuated NF-κB activation in RAW 264.7 cells (online-only Figure III). Because proliferation of PASMCs is increased in animals and humans with PAH, effects of pitavastatin and pitavastatin-NP were examined in human PASMCs in vitro. Treatment with pitavastatin-NP, but not with pitavastatin only, attenuated the proliferation of PASMCs (online-only Figure IV).

Table. Pitavastatin Concentrations in the Lung and Systemic Blood After Intratracheal Administration of Pitavastatin (100 μg per Animal) Only or Pitavastatin-NP Containing the Same Dose of Pitavastatin

	Time After Administration, h					
Groups	1	3	6	12	24	48
Pitavastatin-only group						
Lung, ng/g	115±83	49±69	7±5	2±1	3±3	4±3
Serum, ng/mL	48±19	24±10	9±7	1±1	1±1	1±1
Pitavastatin-NP group						
Lung, ng/g	155±77	17±8	13±13	4±6	7±4	3±1
Serum, ng/mL	65±19	20±5	7±4	2±1	1±1	1±2

Data are mean±SEM (n=6 per group).

Effects of Pitavastatin-NP on Expression of Proinflammatory Factors

As previously reported,[12] MCT-induced PAH was associated with increased gene expression of proinflammatory factors. Intratracheal treatment with pitavastatin-NP significantly reduced the increased gene expression of monocyte chemotactic protein-1, tumor necrosis factor-α, and IL-6 and tended to decrease the expression of IL-1β and intercellular adhesion molecule-1 (online-only Figure V).

Effects of Pitavastatin-NP on eNOS and iNOS Expression

Because the protective effects of statins on PAH have been reported to be attributable at least to the eNOS-related pathway,[11] eNOS protein expression in the lungs was examined on days 3 and 21 after treatment. Western blot analysis showed that MCT administration had no significant effect on eNOS expression on days 3 and 21, compared with untreated controls (Figure 5). Pitavastatin-NP, but not FITC-NP or pitavastatin alone, increased the protein expression of eNOS on day 3, whereas pitavastatin-NP showed no therapeutic effects on eNOS expression on day 21 (Figure 5).

In contrast, iNOS is known to cause oxidant tissue injury and accelerates the pathologic processes of PAH.[21] Immuno-

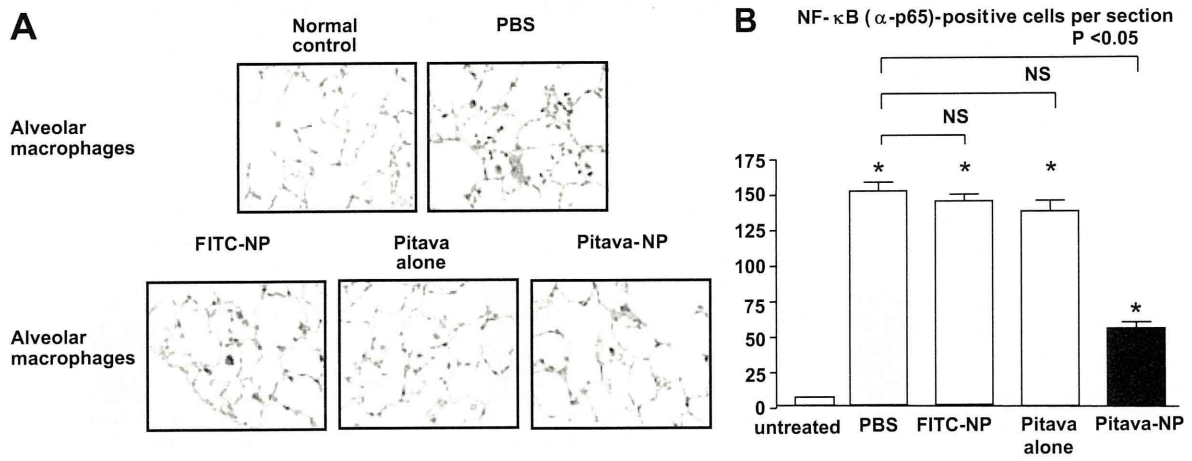

Figure 4. Effects of pitavastatin (pitava)-NP on NF-κB activation. A, Photomicrographs of cross sections of lung stained immunohistochemically with NF-κB (α-p65) from normal rats and PAH rats 3 days after MCT injection. B, Effects of pitavastatin-NP on infiltration of NF-κB (α-p65)–positive cells 3 days after MCT injection. Data are mean±SEM (n=6 per group). *$P<0.01$ vs untreated control.

histochemical expression of iNOS was not detected in lung sections from untreated control rats. Immunostaining for iNOS was noted mainly in alveolar macrophage and weakly in PA lesions 3 days after MCT administration (online-only Figure VI). Single intratracheal instillation of pitavastatin-NP, but not of FITC-NP or pitavastatin only, markedly attenuated the increase in iNOS activity induced by MCT injection.

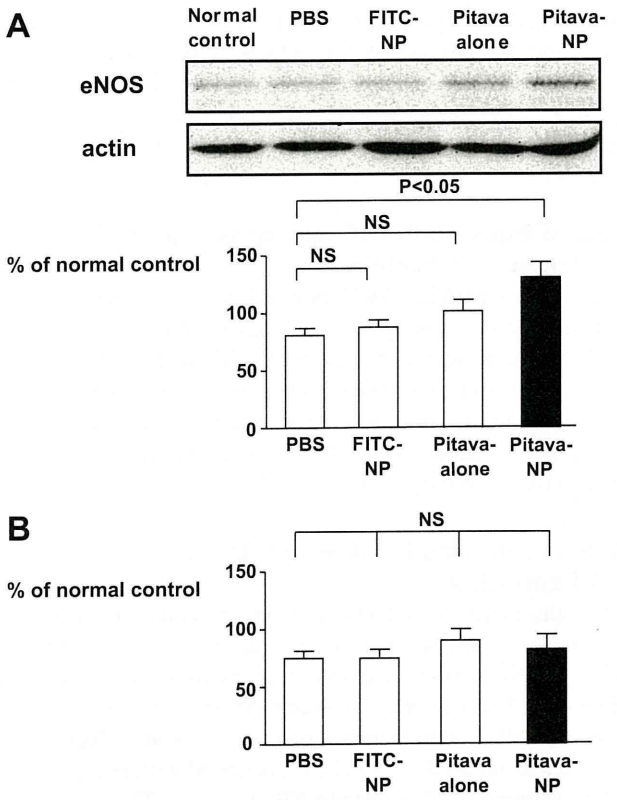

Figure 5. Effects of pitavastatin (pitava)-NP on eNOS protein expression. A, eNOS expression in the lung 3 days after MCT injection. The eNOS level is shown as a percentage of the internal-control actin level. n=6 per group. B, eNOS expression in the lung 21 days after MCT injection. The eNOS level is shown as a percentage of the internal-control actin level. n=6 per group.

Effects of Pitavastatin-NP on Survival

In the treatment protocol, pitavastatin-NP significantly improved survival rate: 42% in the PBS group (n=40), 39% in the FITC-NP group (n=33), 40% in the pitavastatin-alone group (n=40), and 64% in the pitavastatin-NP group (n=58; Figure 6). In addition, pitavastatin-NP caused regression of MCT-induced PAH (Figure 6).

Discussion

We recently reported that intratracheal instillation of a polyethylene glycol-*block*-PLGA copolymer (PEG-PLGA) is an excellent system for drug delivery to the lung.[12] We found in the present study that PLGA NPs were as effective as PEG-PLGA NPs as an NP-mediated drug delivery system to the lung. As we reported with PEG-PLGA NPs,[12] the FITC signals were detected in small bronchial tracts, alveolar macrophages, and small PAs for up to 14 days after a single instillation of FITC-encapsulated PLGA NP.

Statins are known to ameliorate the effects of endothelial injury/dysfunction by enhancing the activity of eNOS and thus, exert multiple vasculoprotective effects on other cell types (vascular smooth muscle cells, monocytes, etc).[3–5] We recently reported that NP-mediated pitavastatin delivery to the vascular endothelium of ischemic skeletal muscles effectively increased therapeutic neovascularization in a murine model of hindlimb ischemia.[13] In our previous study, the beneficial effects of pitavastatin-NP were mediated by increased activity of eNOS.[13] Notably, NP-mediated delivery of pitavastatin had greater angiogenic activity in human endothelial cells in vitro compared with pitavastatin alone.[13] We therefore hypothesized that eNOS and downstream pathogenetic factors might be involved in the therapeutic effects of NP-mediated pitavastatin delivery on MCT-induced PAH. Among statins, pitavastatin was selected as the nanoparticulation compound because this drug elicited the most potent angiogenic effects in human endothelial cells[14] and the most

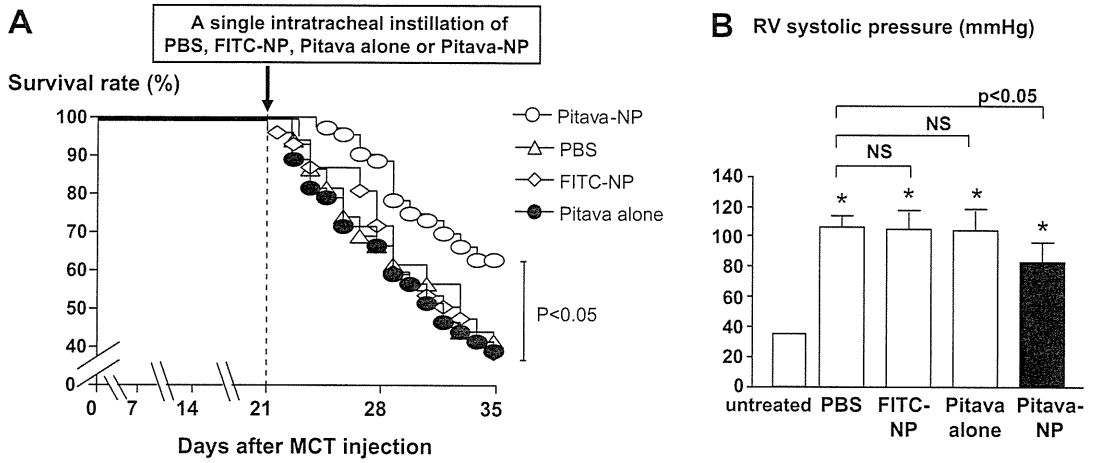

Figure 6. Effects of pitavastatin (pitava)-NP on RV systolic pressure and survival rate. A, Survival curves analyzed by the Kaplan-Meier method in PBS, FITC-NP, pitavastatin only, and pitavastatin-NP groups. B, RV systolic pressure (in mm Hg) in the 4 experimental groups 2 weeks after treatment (at week 5 after MCT injection).

potent inhibitory effects on human PASMC proliferation (Figure 2) in vitro compared with other statins. We also found that NP-mediated intracellular delivery of pitavastatin showed greater inhibitory effects on PASMC proliferation and on NF-κB activation in a monocyte cell line (RAW 264.7 cells) compared with pitavastatin alone (online-only Figures III and IV). Collectively, these in vitro data suggest that NP-mediated pitavastatin delivery is more effective than pitavastatin in inhibiting PASMC proliferation and monocyte activation and improving the deleterious effects of endothelial injury/dysfunction.

The important novel finding of the present study is that a single intratracheal instillation of pitavastatin-NP attenuated the development of PAH (increased RV pressure, PA resistance, and PA remodeling) associated with reduced activity of NF-κB and NF-κB–dependent inflammatory factors (for example, monocyte chemotactic protein-1, IL-1, tumor necrosis factor-α, iNOS, etc). In contrast, eNOS expression was not reduced in the PBS group but was increased by day 3 only but not by day21 (Figure 5), suggesting that eNOS plays a minor role in the therapeutic effects of pitavastatin-NP. Intratracheal instillation of pitavastatin alone at the same dose had no therapeutic effect. Concentrations of pitavastatin in the lungs and systemic blood were found to be similar between animals treated with pitavastatin-NP and those treated with pitavastatin only (the Table). These findings suggest a specific advantage of NP-mediated delivery of pitavastatin to induce therapeutic effects. Therefore, the beneficial effects of pitavastatin-NP on MCT-induced PAH in vivo can be attributable to the pleiotropic effects of pitavastatin-NP, including inhibition of inflammation and cell proliferation.

Prior studies have reported that daily oral administration of statins at high doses beyond the clinical norm (a regimen that could lead to serious adverse side effects in a clinical setting) attenuates MCT- and hypoxia-induced PAH in animals.[7–9] We thus examined whether NP-mediated pitavastatin delivery would be superior to daily oral administration of pitavastatin alone in inhibiting MCT-induced PAH, and we found that oral daily administration of pitavastatin at 0.3 mg/kg per day for 21 days (cumulative dose=25.2 mg per animal, assuming the body weight of animals to be 250 g) had no therapeutic effects, but the same regimen of pitavastatin at 1, 3, and 10 mg/kg per day (cumulative doses=84, 252, and 840 mg per animal, respectively) did show significant therapeutic effects. Therefore, our NP-mediated delivery system (single injection of 0.1 mg pitavastatin per animal) seems to be as effective at an ≈840-times lower dose than the cumulative systemic dose.

It is noteworthy that a single intratracheal treatment with pitavastatin-NP 3 weeks after MCT injection induced regression of PAH and improved survival rate. This finding is more clinically significant than is the mere prevention of PAH. These results suggest that this NP-mediated delivery of pitavastatin may have beneficial therapeutic effects in patients with established PAH.

Perspectives

This mode of NP-mediated delivery of pitavastatin into the lungs is more effective in attenuating the development of MCT-induced PAH compared with intratracheal treatment with pitavastatin alone or systemic administration of pitavastatin, and treatment with pitavastatin-NP induced regression of established PAH. For translation of our present findings into clinical medicine, more clinical studies are needed to investigate whether pitavastatin-NP by inhalation might be effective in improving PAH.

Source of Funding

This study was supported by Health Science Research grants (Research on Nano-medicine and on Intractable Diseases) from the Ministry of Health Labor and Welfare, Tokyo, Japan.

Disclosures

Dr Egashira holds a patent on the results reported in this study. The remaining authors report no conflicts of interest.

References

1. Farber HW, Loscalzo J. Pulmonary arterial hypertension. *N Engl J Med.* 2004;351:1655–1665.
2. Humbert M, Sitbon O, Simonneau G. Treatment of pulmonary arterial hypertension. *N Engl J Med.* 2004;351:1425–1436.